Dynamics and Phase Transitions in Spin-Crossover Complexes: Detailed Nature of Phase Transitions in the Solvate Series $[Fe(3\text{-}OEt\text{-}SalAPA)_2](ClO_4)\cdot S$†

Andrew J. Conti,[1] Kazutoshi Kaji,[2] Yatsuhisa Nagano,[2] Kathryn M. Sena,[1] Yohko Yumoto,[2] Raj K. Chadha,[1] Arnold L. Rheingold,[3] Michio Sorai,*[,2] and David N. Hendrickson*[,1]

Department of Chemistry-0506, University of California at San Diego, La Jolla, California 92093-0506, Microcalorimetry Research Center, Faculty of Science, Osaka University, Toyonaka, Osaka 560, Japan, and Department of Chemistry, University of Delaware, Newark, Delaware 19716

Received July 22, 1992

The detailed nature of the spin-crossover phenomenon and phase transitions observed for the $[Fe(3\text{-}OEt\text{-}SalAPA)_2](ClO_4)\cdot S$ (S is C_6H_6, C_6H_5Cl, C_6H_5Br or $o\text{-}C_6H_4Cl_2$) series is examined. The data base from the preceding paper together with an analysis of the crystal packing, variable-temperature solid-state ^2H NMR data for C_6D_6, C_6D_5Cl and C_6D_5Br solvates, and 13–300 K adiabatic calorimetry data are employed. Four different phases are found for the 3-OEt solvate complexes. Although they have the same basic packing arrangement, $[Fe(3\text{-}OEt\text{-}SalAPA)_2](ClO_4)$ exhibits one other phase for a total of five phases. In all cases there are stacks of Fe^{III} cations surrounded by columns of ClO_4^- anions and S solvate molecules. The 3-OEt benzene solvate gives ΔC_P versus temperature data where there are two smaller sharp peaks at 187 and 295 K superimposed on a broad peak. In the ΔC_P data for the 3-OEt/C_6H_5Cl complex there is broad peak at ~177 K, followed by a very sharp peak at 188.4 K. The C_6H_5Br complex shows a broad ΔC_P peak at ~160 K with a very sharp peak at 288.3 K. For the $o\text{-}C_6H_4Cl_2$ complex, two broad ΔC_P peaks are seen at ~110 and ~150 K with a small sharp peak at 226 K. From X-ray diffraction data it is shown that the C_6H_5Cl and C_6H_5Br solvates show structural phase transitions at 188.4 and 288.3 K, respectively. In these structural phase transitions half of the S solvate molecules undergo a reorientation. In the case of the C_6H_5Br solvate there is little cooperativity between the structural phase transition at 288.3 K and the spin-crossover transformation. The latter progresses essentially as an equilibrium process in the solid state. In the case of the C_6H_5Cl solvate, the 188.4 K phase transition cooperatively involves the spin-crossover change as well as the structural change. The shapes of fraction high spin versus temperature curves from susceptibility data and ΔC_P versus temperature data are analyzed to determine the level of cooperativity in the spin-crossover transformation.

Introduction

Spin-crossover complexes in very dilute solutions[4] have a Boltzmann distribution of complexes in the high- and low-spin states, that is, they are involved in a spin-crossover equilibrium.[5] However, in the solid state, intermolecular interactions could be present. Relatively abrupt transformations of complexes from one state to another may occur in a phase transition. For several years it has been noted[6] that spin-crossover complexes in the solid state make their spin-state transformations in a variety of ways. Some convert abruptly in less than 10 deg from the whole sample being low-spin to the whole sample being high-spin. Other complexes take 100–200 deg of temperature change to make the same conversion. The behaviors of most of the spin-crossover complexes fall somewhere in between these two extremes. However, there has been a tendency[6b] to identify spin-crossover complexes as having either "continuous" or "discontinuous" transformations, where the latter term refers only to those exhibiting an abrupt transformation in a narrow (<10 deg) range.

In addition to variable-temperature X-ray structural characterizations, calorimetric measurements are very useful in determining whether or not a complex makes its transformation in a phase transition. Adiabatic calorimetry measurements have been reported for $Fe(phen)_2(NCS)_2$,[7] $Fe(phen)_2(NCSe)_2$,[7] $[Fe(2\text{-}pic)_3]Cl_2\cdot EtOH$,[8] and $[Fe(acpa)_2]PF_6$,[9] where 2-pic is 2-picolylamine and Hacpa is *N*-(1-acetyl-2-propylidene)(2-pyridylmethyl)amine. The first three Fe^{II} complexes exhibit relatively abrupt spin-crossover transformations. The transformation for the Fe^{III}acpa- complex is gradual. However, all four complexes exhibit well-resolved heat capacity peaks arising from phase transitions. Also, in each case the total entropy gain involved in the phase transition reflects not only the change in electronic entropy ($\Delta S = R \ln 5$ for the $^1A_1$ to $^5T_2$ conversion) but also appreciable local and crystal phonon contributions. For $[Fe(2\text{-}pic)_3]Cl_2\cdot EtOH$ two closely spaced heat-capacity peaks were seen,[8] the presence of which has been analyzed in theoretical models.[10] These two heat capacity peaks may also reflect an onset of motion associated with the EtOH solvate molecule which has been characterized[11] by X-ray crystallography to be involved in a hydrogen-bonding network with the Fe^{II} cations and the Cl^- anions. ^{57}Fe Mössbauer spectroscopy and magnetic susceptibility measurements have demonstrated[12] the presence of two nearby phase transitions in

† The calorimetric part of this paper corresponds to Contribution No. 52 from the Microcalorimetry Research Center.

(1) University of California at San Diego.
(2) Osaka University.
(3) University of Delaware.
(4) There is clear evidence of ion aggregation of spin-crossover complexes and resultant changes in properties in a variety of solvents at concentrations of ~10^{-3} M, see: Conti, A. J.; Xie, C.-L.; Hendrickson, D. N. *J. Am. Chem. Soc.* **1989**, *111*, 1171.
(5) (a) Beattie, J. K. *Adv. Inorg. Chem.* **1988**, *32*, 1. (b) Gütlich, P. *Struct. Bonding (Berlin)* **1981**, *44*, 83.
(6) (a) Rao, C. N. R. *Int. Rev. Phys. Chem.* **1985**, *4*, 19. (b) König, E. *Prog. Inorg. Chem.* **1987**, *35*, 527–622. (c) König, E.; Ritter, G.; Kulshreshtha, S. K. *Chem. Rev.* **1985**, *85*, 219.
(7) (a) Sorai, M.; Seki, S. *J. Phys. Soc. Jpn.* **1972**, *33*, 575. (b) Sorai, M.; Seki, S. *J. Phys. Chem. Solids* **1974**, *35*, 555.
(8) Kaji, K.; Sorai, M. *Thermochim. Acta* **1985**, *88*, 185.
(9) Sorai, M.; Maeda, Y.; Oshio, H. *J. Phys. Chem. Solids* **1990**, *51*, 941.
(10) (a) Sasaki, N.; Kambara, T. *Phys. Rev. B: Condens. Matter* **1989**, *40*, 2442. (b) Jakobi, R.; Spiering, H.; Gütlich, P. *J. Phys. Chem. Solids* **1992**, *53*, 267.
(11) (a) Katz, B. A.; Strouse, C. E. *J. Am. Chem. Soc.* **1979**, *101*, 6214. (b) Mikami, M.; Konno, M.; Saito, Y. *Chem. Phys. Lett.* **1979**, *63*, 566. (c) Mikami, M.; Konno, M.; Saito, Y. *Acta Crystallogr., Sect B* **1980**, *36*, 275.
(12) Petrouleas, V.; Tuchagues, J.-P. *Chem. Phys. Lett.* **1987**, *137*, 21–25.

0020-1669/93/1332-2681$04.00/0

a second Fe^{II} complex. The presence of phase transitions have also been noted[13] for three other spin-crossover complexes with DSC data.

Quite a large number of theoretical models have been developed to explain the characteristics of spin-crossover complexes in the solid state.[14-20] In analogy to ideal solutions it was assumed in earlier theories that in the solid state there is a homogeneous statistical distribution of high- and low-spin complexes. Slichter and Drickamer[15] used a parameter to gauge intermolecular interactions between nearest-neighbor high-spin complexes. In one of the earliest theoretical models Chestnut parameterized intermolecular interactions with a lattice strain parameter. Kambara and Sasaki[18] also employed a lattice strain parameter to couple Jahn–Teller distorted spin-crossover complexes. They were able to simulate observed temperature- and pressure-dependent high-spin fractions as well as the effect of cocrystallizing the iron spin-crossover complex with a complex of another metal. Zimmermann and König[19] introduced the phonon contribution of the lattice by a Debye model with an interpolated Debye temperature. Finally, Spiering *et al.*[20] developed a theory based on the observation that the volumes of the high- and low-spin complexes are different. Again, as with the other theories already mentioned a homogeneous distribution of high- and low-spin complexes was assumed to be present. In the Spiering model complex molecules are coupled with each other via the spin-transition-induced lattice expansion.

In interpreting the heat capacity data for the abrupt transitions in $Fe(phen)_2(NCS)_2$ and $Fe(phen)_2(NCSe)_2$ Sorai and Seki[7] employed the Frenkel theory of heterophase fluctuations.[21] Separate domains of high-spin and low-spin complexes were assumed to be present with strong intermolecular interactions within each domain. Sorai and Seki calculated that in the region of the abrupt phase transition the domain sizes for the two complexes are 95 and 77 molecules, respectively. The idea of separate domains of high-spin and low-spin complexes is obviously a consequence of the nucleation and growth mechanism of phase transitions.[22] Domain structure has been directly seen in phase transitions involving extended magnetic exchange interacting metal centers,[23] as well as in other cooperative phenomena.[24]

In the present paper we examine the factors which control the abruptness of the spin-crossover transformation in the solvate series $[Fe(3\text{-}OEt\text{-}SalAPA)_2](ClO_4)\cdot S$. From the data presented in the preceding paper it is clear that there are several different phases present in these complexes. Which phase is present depends on which solvate molecule S is present and on the temperature. In this paper heat capacity data are reported for four of the solvated complexes in the series, as determined by adiabatic calorimetry. Detailed solid-state ^2H NMR results are also described to examine whether the solvate molecules S convert from static to dynamic at the various phase transitions. Finally, intermolecular contacts present in the different phases are delineated in an effort to develop a phase diagram for the above series of solvated spin-crossover complexes.

Experimental Section

Solid-State ^2H NMR Spectroscopy. Benzene-d_6, chlorobenzene-d_5, and bromobenzene-d_5 were purchased from Aldrich and used without further purification. Deuterated solvate samples were made by dissolving ~50 mg of $[Fe(3\text{-}OMe\text{-}SalAPA)_2](ClO_4)$ in ~20–25 mL of spectral grade CH_2Cl_2 (Aldrich). This solution was filtered and to this stirred solution was added dropwise ~5–15 mL of one of the above deuterated solvents. Polycrystalline samples of $[Fe(3\text{-}OMe\text{-}SalAPA)_2](ClO_4)\cdot S$ were obtained in 1–3 days by slow evaporation. The samples were mildly ground to ensure that a powder distribution was obtained.

Solid-state ^2H NMR quadrupole-echo spectra were obtained on a 55.3-MHz home built spectrometer of conventional design. A 10-mm long solenoid sample coil was used, which accommodates short sections of 5-mm NMR tubes. The 90° pulse length delivered by a ENT LPI-10 linear pulse amplifier was 1.8 μs. Spectra were obtained by using the standard 90_x–τ–90_y–acquire sequence with $\tau = 30$ μs and an eight phase cycle to suppress artifacts. A Nicolet digital oscilloscope was used for data acquisition with a dwell time of 0.2 μs at all temperatures. A total of ~14 000 transients were collected for each spectrum run at the higher temperatures, whereas only ~4500 transients were needed for the low-temperature data collection. Raw echo decays were transferred to an off-line computer for processing with a software package from Hare Research, Inc. Line-shape simulations were performed with the program MXET1, which is a modified form of a previously described program MXQET.[25] The program MXET1 was used to simulate spectra on a Silicon Graphics Iris workstation.

Heat Capacity Measurements. An adiabatic calorimeter[26] was employed to measure the heat capacity from 13 to 320 K for the C_6H_6, C_6H_5Cl, C_6H_5Br, and $o\text{-}C_6H_4Cl_2$ solvates. In one experiment a calorimeter cell[27] made of gold-plated copper was loaded with 16.4339 g (0.0225726 mol) of polycrystalline $[Fe(3\text{-}OEt\text{-}SalAPA)_2](ClO_4)\cdot C_6H_6$ with a buoyancy correction using the density of 1.34 g cm^{-3}.[28] A small amount of helium gas was sealed in the cell to aid the heat transfer. In separate experiments quantities of 16.8747 g (0.0221310 mol), 18.7807 g (0.0232739 mol), and 17.1848 g (0.0215636 mol) of the C_6H_5Cl, C_6H_5Br, and $o\text{-}C_5H_4Cl_2$ solvates, respectively, were loaded into the calorimeter cell, where the buoyancy corrections were based upon the crystal densities (1.45, 1.46, and 1.44 g cm^{-3}, respectively) determined in the X-ray structures.[29]

Vibrational Spectroscopies. Variable-temperature IR spectra for all four solvates were recorded for Nujol mulls between 88 and 300 K with a Japan Spectroscopic Co. Model DS-402G infrared spectrophotometer in the range of 400–4000 cm^{-1}. A Hitachi Model FIS-3 far-infrared spectrometer was employed to run variable-temperature spectra in the 30–400 cm^{-1} range. Multi-temperature (84–294 K) Raman spectra in the range of 80–1000 cm^{-1} were recorded for KBr disks with Japan Spectroscopic Co. spectrophotometer using the 514.5-nm line from an Ar laser.

Results and Discussion

Heat Capacity Results. Adiabatic calorimetry measurements from 13 to 320 K were made for the four $[Fe(3\text{-}OEt\text{-}SalAPA)_2](ClO_4)\cdot S$ compounds where S is either C_6H_6, C_6H_5Cl, C_6H_5Br, or $o\text{-}C_6H_4Cl_2$. In Figure 1 is shown a plot of the molar heat capacity at constant pressure, C_P, versus temperature for the benzene solvate complex. In Figure 1 there is a broad anomaly which begins at ~120 K with a peak at 187 K. Compared to

(13) (a) Kulshreshtha, S. K.; Iyer, R. M.; König, E.; Ritter, G. *Chem. Phys. Lett.* **1984**, *110*, 201. (b) Kulshreshtha, S. K.; Iyer, R. M. *Chem. Phys. Lett.* **1984**, *108*, 501.
(14) Chestnut, D. B. *J. Chem. Phys.* **1964**, *40*, 405.
(15) Slichter, C. P.; Drickamer, H. G. *J. Chem. Phys.* **1972**, *56*, 2142.
(16) Bari, R. A.; Sivardiere, J. *Phys. Rev. B* **1972**, *5*, 4466.
(17) Wajnflasz, J. *Phys. Status Solidi* **1970**, *40*, 537.
(18) (a) Kambara, T. *J. Chem. Phys.* **1979**, *70*, 4199. (b) Sasaki, N.; Kambara, T. *J. Chem. Phys.* **1981**, *74*, 3472. (c) Kambara, T. *J. Chem. Phys.* **1981**, *74*, 4557. (d) Kambara, T. *J. Phys. Soc. Jpn.* **1980**, *49*, 1806. (e) Ogata, F.; Kambara, T.; Sakaki, N.; Gondaira, K. I. *J. Phys. C: Solid State Phys.* **1983**, *16*, 1391. (f) Kambara, T. *J. Phys. Soc. Jpn.* **1981**, *50*, 2257. (g) Ogata, F.; Kambara, T.; Gondaira, K. I.; Sasaki, N. *J. Magn. Magn. Mater.* **1983**, *31–34*, 123.
(19) (a) Zimmermann, R.; König, E. *J. Phys. Chem. Solids* **1977**, *38*, 779. (b) Zimmermann, R. *J. Phys. Chem. Solids* **1983**, *44*, 151.
(20) (a) Spiering, H.; Meissner, E.; Köppen, H.; Müller, E. W.; Gütlich, P. *Chem. Phys.* **1982**, *68*, 65. (b) Adler, P.; Wiehl, L.; Meissner, E.; Köhler, C. P.; Spiering, H.; Gütlich, P. *J. Phys. Chem. Solids* **1987**, *48*, 517.
(21) Frenkel, J. In *Kinetic Theory of Liquids*; Oxford University Press: London, 1947; Chapter VII.
(22) Rao, C. N. R.; Rao, K. J. *Phase Transitions in Solids*; McGraw-Hill Inc.: New York, 1978.
(23) *Magnetic Oxides, Part 2 and 2*; Craik, D. J., Ed.; John Wiley & Sons: New York, 1975.
(24) Domain structure has been directly seen for compounds undergoing phase transitions involving the cooperative Jahn–Teller effect, see: Gehring, G. A.; Gehring, K. A. *Rep. Prog. Phys.* **1975**, *38*, 1.
(25) (a) Greenfield, M. S.; Ronemus, A. D.; Vold, R. L.; Vold, R. R.; Ellis, P. D.; Raidy, T. R. *J. Magn. Reson.* **1987**, *72*, 89. (b) Ronemus, A. D. Ph.D. Dissertation, University of California, San Diego, 1987.
(26) Sorai, M.; Kaji, K.; Kaneko, Y. *J. Chem. Thermodyn.* **1992**, *24*, 167.
(27) Ogasahara, K.; Sorai, M.; Suga, H. *Mol. Cryst. Liq. Cryst.* **1981**, *71*, 189.
(28) Timken, M. D.; Strouse, C. E.; Soltis, S. M.; Daverio, S. A.; Hendrickson, D. N.; Abdel-Mawgoud, A. M.; Wilson, S. R. *J. Am. Chem. Soc.* **1986**, *108*, 395.
(29) Conti, A. J.; Chadha, R. K.; Sena, K. M.; Rheingold, A. L.; Hendrickson, D. N. *Inorg. Chem.*, preceding paper in this issue.

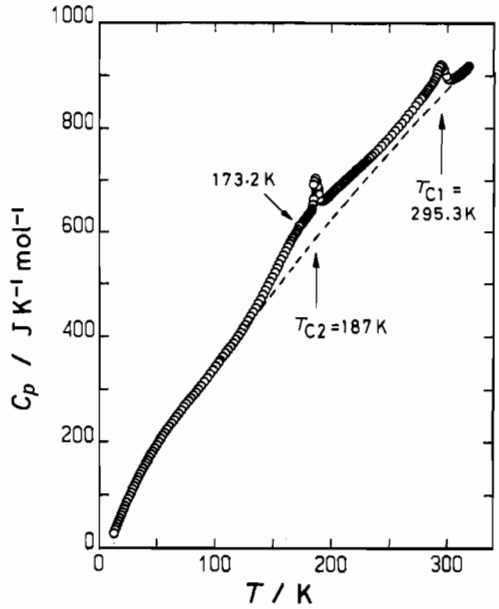

Figure 1. Plot of the molar heat capacity at constant pressure, C_P, versus temperature for [Fe(3-OEt-SalAPA)$_2$](ClO$_4$)·C$_6$H$_6$. The dashed line shows the lattice heat capacity evaluated by an effective frequency distribution method.

the "normal" heat capacity, excess heat capacity is still present at temperatures above the 187 K peak. In fact, as the temperature is increased above 187 K a second C_P peak is encountered at 295 K.

In order to determine the excess heat capacity due to phase transitions involving the spin-crossover phenomenon and other structural changes it is necessary to estimate the "normal" heat capacity curve, *i.e.*, a lattice heat capacity, C_{lat}. An effective frequency distribution method[30] was used for the benzene solvate. The normal heat capacity of a solid reflects both a continuous acoustic phonon distribution and many discrete optical branches corresponding to intramolecular vibrational modes. Modes which cannot be assigned are included in a continuous phonon distribution and an effective frequency distribution spectrum is obtained by least-squares fitting to the observed heat capacities. The frequencies of many, but not all, of these fundamental vibrational modes can be extracted from IR (30–4000 cm^{-1}) and Raman (80–1000 cm^{-1}) data. When the sample temperature is increased, several bands which belong to complexes in the high-spin state gain intensity at the expense of bands attributable to complexes in the low-spin state.

To get the normal lattice heat capacity for the benzene solvate it was necessary to determine independently the normal lattice heat capacity curves for the low-spin state, C_{lat}(LS), and for the high-spin state, C_{lat}(HS). The details of how this was done are given in a separate paper.[31] Suffice it to say, the normal heat-capacity curve, C_{lat}, for a spin-crossover complex is given as

$$C_{lat} = f_{HS}C_{lat}(HS) + (1 - f_{HS})C_{lat}(LS) \quad (1)$$

In this equation f_{HS} is the high-spin fraction. The temperature dependence of f_{HS} was evaluated with the magnetic susceptibility data given for the benzene solvate in the preceding paper. The observed magnetic moment follows eq 2.

$$\mu_{eff}^2 = f_{HS}\mu_{eff}^2(HS) + (1 - f_{HS})\mu_{eff}^2(LS) \quad (2)$$

In Figure 1 the dashed line represents the normal lattice heat capacity estimated as described above for [Fe(3-OEt-SalAPA)$_2$](ClO$_4$)·C$_6$H$_6$. After subtracting this normal lattice heat capacity from the observed C_P values the excess heat capacity

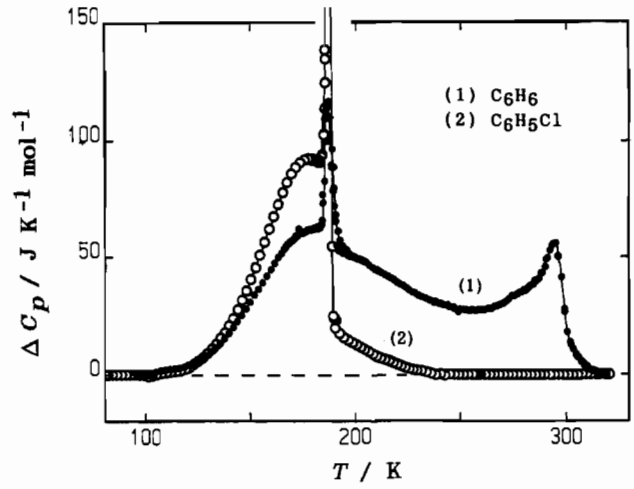

Figure 2. Plot of the excess heat capacity, ΔC_P, versus temperature for [Fe(3-OEt-SalAPA)$_2$](ClO$_4$)·C$_6$H$_6$ (●) and [Fe(3-Oet-SalAPA)$_2$](ClO$_4$)·C$_6$H$_5$Cl (○).

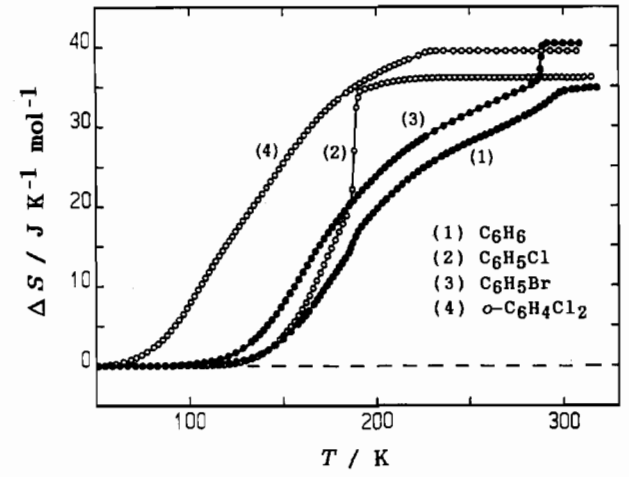

Figure 3. Plot of entropy gain, ΔS, versus temperature for the four solvates [Fe(3-OEt-SalAPA)$_2$](ClO$_4$)·S where the solvate molecules S is (1) C$_6$H$_6$, (2) C$_6$H$_5$Cl, (3) C$_6$H$_5$Br, and (4) o-C$_6$H$_4$Cl$_2$.

associated with phase transitions, ΔC_P, is obtained. In Figure 2 is given a plot of ΔC_P versus temperature for the benzene solvate. The total enthalpy change, ΔH, and total entropy change, ΔS, associated with the phase transitions (*i.e.*, throughout the whole temperature range where there is excess heat capacity) of the benzene solvate were determined by integration of ΔC_P with respect to T and ln T, respectively. The total integration values were calculated to be ΔH = 7080 J mol^{-1} and ΔS = 34.8 J K^{-1} mol^{-1}. In Figure 3 is given a plot of ΔS versus temperature for [Fe(3-OEt-SalAPA)$_2$](ClO$_4$)·C$_6$H$_6$.

A careful examination of Figures 2 and 3, together with other facts, suggests that the benzene solvate undergoes two phase transitions, one at 187 K and the other at 295 K. The X-ray structure of the benzene solvate was determined[28] at 20, 128, 175, 298, and 300 K. At the first three temperatures the space group was found to be $P2_1/c$, while at 298 and 300 K the space group is $C2/c$. The intensities of the (–5,–2,1) reflection and three symmetry-related reflections were also monitored as the temperature was increased from 20 to 225 K. These reflections are systematically absent in $C2/c$. A gradual decrease in average intensity was noted in the 80–150 K range. An abrupt decrease (~60–80% in ~20 deg) in intensity was seen above 180 K. In fact, a marked hysteresis (ΔT = 15 K) was taken[28] to indicate the presence of a significant first-order component to the phase transition. These crystallographic studies were reported[28] before the C_P data were measured. After the C_P data were in hand and it was known that there are two phase transitions at 187 and 295

(30) Sorai, M.; Seki, S. *J. Phys. Soc. Jpn.* **1972**, *32*, 382.
(31) Kaji, K.; Sorai, M.; Conti, A. J.; Hendrickson, D. N. *J. Phys. Chem. Solids*, in press.

K, additional crystallographic studies were carried out.[32] When a crystal was cooled below the 295 K phase transition, it was found that the diffraction peaks reversibly split into multiplets, indicative of internal twinning (*i.e.*, domain structure). When the crystal was cooled below 150 K and annealed for several hours and then warmed to 200 K, diffraction peaks had reasonable mosaic spreads. However, even after a full data set was collected, it was not possible to characterize definitively what structural changes occurred at the 187 K phase transition.

Heat capacity data were collected for [Fe(3-OEt-SalAPA)$_2$](ClO$_4$)·C$_6$H$_5$Cl. The normal heat capacity curves for this compound and the other two solvates were constructed by an extrapolation technique, the details of which will be presented in separate papers.[33] In Figure 2 is given a plot of ΔC_P versus temperature. Similar to the benzene solvate, excess heat capacity first appears at ~100 K as the C$_6$H$_5$Cl solvate is heated. There is a broad peak in ΔC_P at ~177 K, followed by a very sharp maximum in ΔC_P at 188.4 K. Furthermore, at a temperature immediately above this phase transition ΔC_P falls abruptly to a value near to the normal lattice heat capacity. In Figure 3 is given a comparison of ΔS versus temperature for the C$_6$H$_6$ and C$_6$H$_5$Cl solvates. The differences are remarkable. Not only is the total entropy gain for the C$_6$H$_5$Cl solvate (ΔS = 36.1 J K^{-1} mol^{-1}) greater than that measured for the C$_6$H$_6$ solvate, the C$_6$H$_5$Cl solvate gains most all of its entropy rather abruptly in one phase transition at 188.4 K. This clearly indicates that whatever is happening in the phase transition of the C$_6$H$_5$Cl solvate there is considerably more cooperativity present for the C$_6$H$_5$Cl solvate than the C$_6$H$_6$ solvate. The total enthalpy gain measured for the C$_6$H$_5$Cl solvate is ΔH = 6340 J mol^{-1}.

There is good evidence that the 188.4 K phase transition of the C$_6$H$_5$Cl solvate involves, in part, the spin-crossover transformation. Variable-temperature magnetic susceptibility data were run for a ~50-mg portion of the large heat capacity sample. Data were collected in both the heating and cooling directions. Little hysteresis was found; however, it was necessary to spend ~0.5 h for temperature equilibration at each point. For the heating data set the plot of μ_{eff} versus temperature looked very similar to that shown in Figure 1 of the preceding paper. The susceptibility data for the heat capacity sample were converted to values of f_{HS} versus temperature. The shape of a plot of ΔC_P versus temperature would reflect an increase in f_{HS} as a function of temperature. In Figure 4 is shown a plot of df_{HS}/dT versus temperature in the phase transition region. It is interesting to see that the shape of the df_{HS}/dT plot looks similar to the ΔC_P versus temperature plot. In both cases there is a broader bump which occurs at a lower temperature than the sharp feature occurring at 188.4 K for the phase transition. It is clear that the spin-crossover transformation is involved in the 188.4 K phase transition. As is discussed later in this paper, the C$_6$H$_5$Cl solvate also experiences a structural change at this same temperature.

Two features are evident in the plot of ΔC_P versus temperature shown in Figure 5 for [Fe(3-OEt-SalAPA)$_2$](ClO$_4$)·C$_6$H$_5$Br. There is a broad thermal anomaly which starts at ~100 K, peaks at ~160 K and seems to run up to the second much more abrupt thermal anomaly at 288.3 K. Integration of the ΔC_P data with respect to T and ln T gives total changes of ΔH = 7990 J mol^{-1} and ΔS = 40.4 J K^{-1} mol^{-1}. A plot of ΔS versus temperature for the C$_6$H$_5$Br solvate is given in Figure 3. The total ΔS (=40.4 J K^{-1} mol^{-1}) for the C$_6$H$_5$Br solvate is comparable to that of the C$_6$H$_5$Cl solvate; however, the temperature dependencies are quite different. The abrupt peak at 288.3 K contributes a ΔS value of ~4.7 J K^{-1}, which is close to the value of R ln 2 (=5.76 J K^{-1} mol^{-1}). Even though the C$_6$H$_5$Cl and C$_6$H$_5$Br solvates seem to interconvert between the same two phases (*vide infra*), it is clear there are pronounced differences between the manners in which they interconvert.

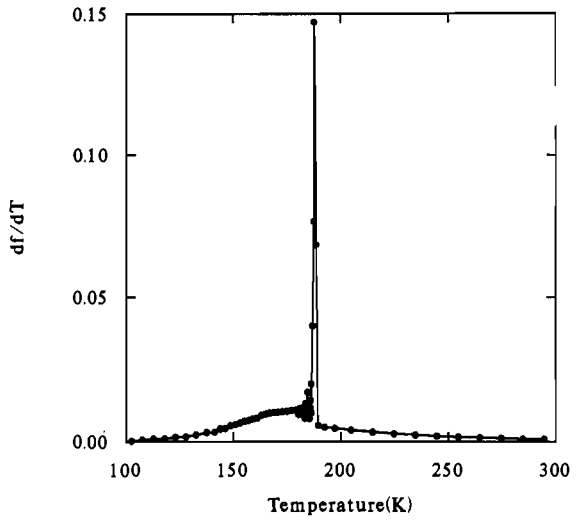

Figure 4. Temperature dependence of the fraction of high-spin complexes, df_{HS}/dT, versus temperature in the region of the 188.4 K phase transition for [Fe(3-OEt-SalAPA)$_2$](ClO$_4$)·C$_6$H$_5$Cl. The fraction of high-spin complexes, f_{HS}, was evaluated from magnetic susceptibility data measured for a portion of the heat-capacity sample.

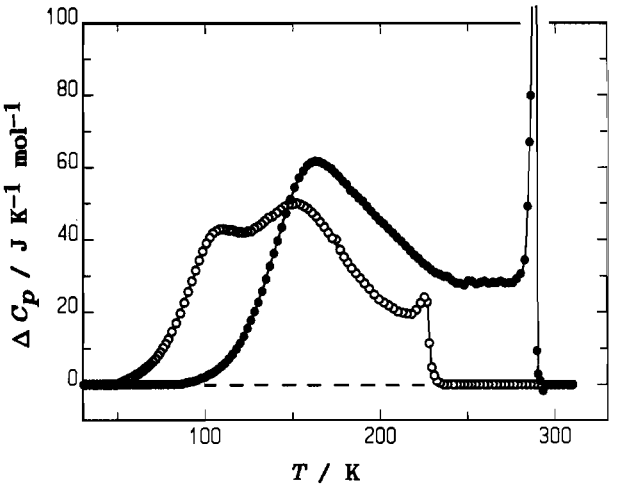

Figure 5. Plot of the excess heat capacity, ΔC_P, versus temperature for [Fe(3-OEt-SalAPA)$_2$](ClO$_4$)·C$_6$H$_5$Br (●) and [Fe(3-OEt-SalAPA)$_2$](ClO$_4$)·*o*-C$_6$H$_4$Cl$_2$ (○).

Table I. Total Enthalpy (ΔH) and Total Entropy (ΔS) Changes Evaluated for the [Fe(3-OEt-SalAPA)$_2$](ClO$_4$)·S Complexes

solvate S	ΔH, kJ/mol	ΔS, J/(K mol)
C$_6$H$_6$	7.08 ± 0.35	34.8 ± 1.5
C$_6$H$_5$Cl	6.34	36.1
C$_6$H$_5$Br	7.99	40.4
o-C$_6$H$_4$Cl$_2$	5.38	39.5

In Figure 5 is given a plot of ΔC_P versus temperature determined for [Fe(3-OEt-SalAPA)$_2$](ClO$_4$)·*o*-C$_6$H$_4$Cl$_2$. Three heat-capacity anomalies can be seen. There is one beginning at ~70 K with a peak at ~110 K. A second broad heat-capacity anomaly peaks at ~150 K. The third anomaly occurs at 226 K and is more abrupt than the other two. Overall the smeared out appearance of the ΔC_P versus temperature plot for the *o*-C$_6$H$_4$Cl$_2$ solvate is not unlike that of the C$_6$H$_6$ solvate (Figure 2). The X-ray structure of the *o*-C$_6$H$_4$Cl$_2$ solvate is only known at ~295 K. In Table I are summarized the total ΔH and ΔS values calculated from the ΔC_P versus temperature data for the C$_6$H$_6$, C$_6$H$_5$Cl, and *o*-C$_6$H$_4$Cl$_2$ solvates. These ΔS values correspond to entropy gains of R ln x, where x is equal to the number of degrees, 65.7, 76.9, 129, and 116, respectively, for the four solvates.

(32) Strouse, C. E. Unpublished results.
(33) (a) Nagano, Y.; Sorai, M.; Conti, A. J.; Hendrickson, D. N. Manuscript in preparation (the C$_6$H$_5$Cl solvate). (b) Yumoto, Y.; Sorai, M.; Conti, A. J.; Hendrickson, D. N. Manuscript in preparation (the C$_6$H$_5$Br solvate). (c) Sorai, M.; Conti, A. J.; Hendrickson, D. N. Manuscript in preparation (the *o*-C$_6$H$_4$Cl$_2$ solvate).

It is clear from the room temperature X-ray structures of the C_6H_5Cl, C_6H_5Br, and o-$C_6H_4Cl_2$ solvates that there is no disorder of the halogen atoms of the solvate molecules. Thus, if the C_6H_5Cl molecule converts in the abrupt phase transition from being static to dynamic in the crystal, it does not rotate about a pseudo-C_6 axis which is perpendicular to the plane of the C_6H_5Cl molecule. The onset of libration about the C_2 axis running through the chlorine atom and the para carbon atom of each C_6H_5Cl molecule is a distinct possibility; however, the onset of this motion would not contribute to ΔS. In addition to the solvate molecules, there are several other parts of these complexes which may convert from static to dynamic in a phase transition. The room-temperature thermal parameters of the ClO_4^- anions in all four complexes are large and could reflect dynamics at room temperature. The room-temperature thermal parameters of the carbon atoms of the ethyl substituents are also large. If each $-OCH_2CH_3$ substituent on the cation converts from being static to dynamically moving between two positions, then there is a contribution to ΔS of $R \ln 2 + R \ln 4$ (=11.53 J K^{-1} mol^{-1}), since there are two ethyl groups per cation. In the range of ~100–300 K there may also be an onset of motion where the two six-membered propylene chelate rings are interconverting between different conformations.

Solid-State ^{2}H NMR Spectroscopy. Perhaps the best technique to gauge which parts of a solid are static or not and whether they experience an onset of dynamics at a phase transition is solid-state ^{2}H NMR spectroscopy.[34] The solvate molecules were deuterated for three of the solvated complexes. Variable-temperature ^{2}H NMR spectra were run for polycrystalline samples of each of these three solvates. There have been a limited number of reportings of ^{2}H NMR studies of paramagnetic compounds.[35] One of the earliest and most definitive was carried out by Soda and Chiba.[35f] The nature of the S solvate molecules has been probed by the solid-state ^{2}H NMR technique for several paramagnetic mixed-valence $Fe_2^{III}Fe^{II}$ μ_3-oxo-bridged complexes of the composition $[Fe_3O(O_2CCH_3)_6(py)_3]S$, where py is pyridine (substituted in some cases) and S is C_6H_6, py, $CHCl_3$, or some other solvate molecule.[36] Solid-state ^{2}H NMR spectroscopy proved uniquely suited to establish that the onset of motion of the solvate molecule is involved in the valence-detrapping phase transitions in these mixed-valence complexes.

The ^{2}H nucleus has a nuclear spin of $I = 1$. For a diamagnetic compound in the solid state, the quadrupolar interaction of the nuclear charge asymmetry and the nearby electronic charge asymmetry dominate the ^{2}H NMR spectrum. In the case of a polycrystalline sample, powder ^{2}H NMR patterns are seen which have characteristic "turning points" (*i.e.*, spectral features) that can be used to assess the quadrupolar interaction. In general a powder pattern for each type of deuteron is characterized by the quadrupole coupling constant $e^2q_{zz}Q/h$ and the asymmetry parameter η, where eQ is the nuclear quadrupole moment and eq_{zz} is the principal component of the electric field gradient associated with the electronic charge distribution about the ^{2}H nucleus. Usually eq_{zz} is directed along the C–D bond vector.

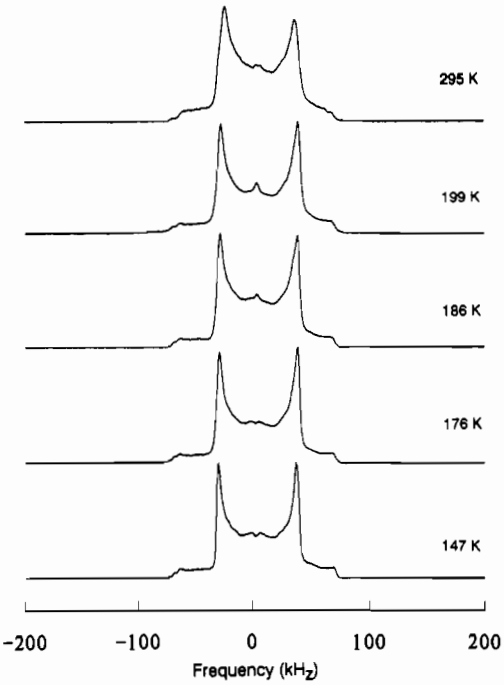

Figure 6. Variable-temperature ^{2}H NMR spectrum for a polycrystalline sample of $[Fe(3\text{-}OEt\text{-}SalAPA)_2](ClO_4)\cdot C_6D_6$.

Table II. Effective Quadrupolar Coupling Constants and Benzene Wobbling Angle Evaluated from ^{2}H NMR Spectra of $[Fe(3\text{-}OEt\text{-}SalAPA)_2]ClO_4\cdot C_6H_6$

T, K	$(e^2q_{zz}Q/h)_{eff}$,[a] kHz	β_0,[b] deg
147	183	0
176	183	0
186	180	7(2)
199	181	7(2)
295	164	22(22)

[a] Effective quadrupolar coupling constant determined by horn-to-horn separation in spectrum. [b] Half-angle characterizing the wobbling of the normal to the plane of the C_6D_5 solvate molecule. The angle β_0 is defined in eq 5.

Also, the quadrupole coupling constant (QCC) is essentially the same value for the ortho-, meta or para-positioned deuterons of a monosubstituted benzene such as C_6D_5Cl. The asymmetry parameter η gauges for each C–D bond the difference in magnitude between the other two components of the electric field gradient as defined in eq 3. The parameter η varies from 0 (axial case)

$$\eta = \frac{q_{yy} - q_{xx}}{q_{zz}} \tag{3}$$

to 1. The line shape for a polycrystalline sample reflects the random distribution of orientations of the electric field gradients of the deuteron with respect to the external magnetic field H_0. Thus, the quadrupole splitting ($\Delta\nu$) for the doublet of a deuteron nucleus depends on the values of the QCC and η parameters as well as the orientation of eq_{zz} as given by eq 4. In this equation

$$\Delta\nu = \frac{3}{4}\left(\frac{e^2q_{zz}Q}{h}\right)(3\cos^2\theta - 1 + \eta\sin^2\theta\cos 2\phi) \tag{4}$$

θ and ϕ are the polar angles which characterize the orientation of eq_{zz} with respect to laboratory coordinates (*i.e.*, direction of H_0). When the part of a molecule where the deuteron is located experiences an onset of motion in a crystal lattice, an appreciable reduction in the quadrupole splitting may be seen.

In Figure 6 are displayed variable-temperature ^{2}H NMR spectra for a polycrystalline sample of $[Fe(3\text{-}OEt\text{-}SalAPA)_2](ClO_4)\cdot C_6D_6$. Parameters measured from these spectra are given in Table II. It can be seen that throughout the 147–295 K region each powder spectrum is essentially axial. A

(34) Fyfe, C. A. *Solid State NMR for Chemists*; C. F. C. Press: Guelph, Ontario, Canada, 1983.
(35) (a) Haw, J. F.; Campbell, G. C. *J. Magn. Reson.* **1986**, *66*, 588. (b) Campbell, G. C.; Crosby, R. C.; Haw, J. F. *J. Magn. Reson.* **1986**, *69*, 191. (c) Chacko, V. P.; Granapathy, S.; Bryant, R. G. *J. Am. Chem. Soc.* **1983**, *105*, 5491. (d) Granapathy, S.; Chacko, V. P.; Bryant, R. G.; Etter, M. C. *J. Am. Chem. Soc.* **1986**, *108*, 3159. (e) Granapathy, S.; Bryant, R. G. *J. Magn. Reson.* **1986**, *70*, 149. (f) Soda, G.; Chiba, T. *J. Chem. Phys.* **1969**, *50*, 439.
(36) (a) Oh, S. M.; Kambara, T.; Hendrickson, D. N.; Sorai, M.; Kaji, K.; Woehler, S. E.; Wittebort, R. J. *J. Am. Chem. Soc.* **1985**, *107*, 5541. (b) Woehler, S. E.; Wittebort, R. J.; Oh, S. M.; Hendrickson, D. N.; Inniss, D.; Strouse, C. E. *J. Am. Chem. Soc.* **1986**, *108*, 2938. (c) Woehler, S. E.; Wittebort, R. J.; Oh, S. M.; Kambara, T.; Hendrickson, D. N.; Inniss, D.; Strouse, C. E. *J. Am. Chem. Soc.* **1987**, *109*, 1063. (d) Oh, S. M.; Wilson, S. R.; Hendrickson, D. N.; Woehler, S. E.; Wittebort, R. J.; Inniss, D.; Strouse, C. E. *J. Am. Chem. Soc.* **1987**, *109*, 1073. (e) Jang, H. G.; Wittebort, R. J.; Sorai, M.; Kaneko, Y.; Nakano, M.; Hendrickson, D. N. *Inorg. Chem.* **1992**, *31*, 2265.

η value of 0.05 has been estimated by simulations for the 147 K spectrum. The slight line-width asymmetry in the 295 K spectrum is likely attributable to the effects of neighboring $S = {}^5/_2$ paramagnetic cations. Since these spectra remain close to axial throughout the temperature region, this indicates that whatever motion is present it is fast or slow compared with the QCC of an aromatic deuteron. The QCC for a static benzene molecule in crystalline benzene has been determined to be 183 kHz.[37] With reference to the 147 K spectrum in Figure 6, this means that for a static benzene molecule with $\eta = 0$ the two sharp perpendicular turning points ("horns") should be separated by 137.2 kHz, whereas the two broader parallel turning points should be separated by 274.5 kHz (calculated with eq 4). The two splittings present in this 147 K spectrum are almost exactly half those expected for a static benzene molecule. It can be concluded that at 147 K the benzene solvate molecule is rapidly rotating about a pseudo-C_6 axis normal to the plane of the molecule. Also, because the X-ray crystallography[28] of the C_6H_6 solvate shows distinct carbon atom positions, this motion must proceed by jumps between relatively deep potential minima rather than by small-step diffusion.

As the temperature of the C_6D_6 solvate is increased (Figure 6) from 147 to 176 K there is little change in the spectrum. A further increase in the temperature to 186 and then 199 K leads to a small but real decrease in the splitting between the two "horns". This decrease in splitting between the "horns" becomes quite evident in increasing the temperature to 295 K. In a very recent study of the ^{2}H NMR spectra of crystalline benzene and of benzene in a cyclamer inclusion host Ok *et al.*[36] noted a similar behavior. For both of these compounds, when the temperature was increased above the point where the benzene molecules are rotating rapidly about their local C_6 axes, they noted a small decrease in $e^2q_{zz}Q/h$ as the temperature was increased. It was shown that this temperature dependence of $e^2q_{zz}Q/h$ could be accounted for by assuming that the benzene ring normal wanders uniformly in a cone of half-angle β_0. Since this wobbling was assumed to be too fast to contribute to the line shape, it leads to a smaller effective QCC given by eq 5. In this equation $(e^2q_{zz}Q/h)_0$ is the QCC for a static C_6D_6 molecule.

$$(e^2q_{zz}Q/h)_{\text{eff}} = (e^2q_{zz}Q/h)_0\ ({}^1/_2)\cos\beta_0\ (1 + \cos\beta_0) \quad (5)$$

Equation 5 was used together with the experimentally determined effective QCC at each temperature and a value of 183 kHz for the QCC of a static benzene to calculate the values of β_0 given in Table II. From the heat capacity and crystallography data it is known that the benzene solvate undergoes a phase transition at 187 K. Throughout the 147–295 K region the NMR data show the C_6D_6 solvate molecules are always rapidly rotating about their local C_6 axes. In heating from 176 K to the 186–199 K region, each C_6D_6 starts to wobble slightly with the β_0 angle increasing to 7(2)° from zero. Finally at 295 K the NMR spectrum shows that each C_6D_6 is rapidly wobbling with an even larger β_0 angle of 22(2)°. Thus, in the 187 K phase transition only a small increase in wobbling of the solvate molecule C_6D_6 is observed. At the 295 K phase transition the wobbling becomes more pronounced. However, in both cases the onset or increase in "wobbling angle" would not contribute to ΔS because one is simply converting from one configuration to another if there are no potential-energy barriers for the wobbling C_6D_6 molecule.

^{2}H NMR spectra obtained for a polycrystalline sample of [Fe(3-OEt-SalAPA)$_2$](ClO$_4$)·C_6D_5Cl are shown in Figure 7. At 168 K the separation between the two 90° turning points is 132 kHz, which corresponds to a QCC of 176 kHz. This value is somewhat less than what has been observed for many monosubstituted benzenes, for which a median value of 181 kHz is found.[36b,37] At 168 K there is already some small amount of motion in the C_6D_5Cl solvate molecules. As the temperature is increased above the abrupt phase transition (Figure 2) at 188.4 K there is not an abrupt change in the ^{2}H NMR spectrum. Somewhere in the 185–198 K region each of the two 90° turning points split into two features. This is a sign that some additional small motion appears in a fraction of the deuteron sites. The carbon and chlorine atoms of the C_6H_5Cl solvate molecules are well defined in the crystallography. The thermal parameters of these atoms are large at 295 K, but not excessive. It is clear that there is no rotation about an axis normal to the ring at any temperature. Probably the only motion of the C_6H_5Cl solvate possible at temperatures below 295 K is about a pseudo-C_2 axis running through the chlorine atom, the carbon atom to which it is attached, and the para carbon atom. However, simulations of the spectrum show that there is not a 180° reorientation about this C_2 axis.

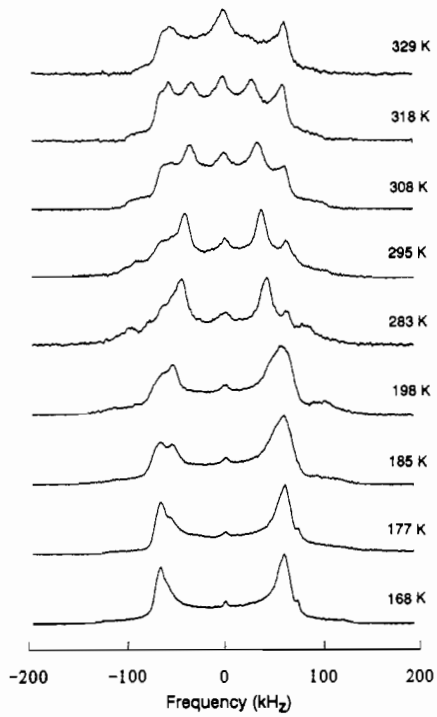

Figure 7. Variable-temperature ^{2}H NMR spectrum for a polycrystalline sample of [Fe(3-OEt-SalAPA)$_2$](ClO$_4$)·C_6D_5Cl.

The temperature dependence of the spectrum of the C_6D_5Cl solvate (Figure 7) is best explained by librational motion about the C_2 axis which runs through the Cl atom. After considerable effort in trying to simulate the spectra it became clear that the motion involved is where the plane of the C_6D_5Cl molecule librates about the C_2 axis. The plane of the molecule moves by an angular displacement of β' degrees, where β' is considerably less than 180°. In addition to the libration angle β', the rate of libration is important for each simulated spectrum. In Figure 8 are given several simulated spectra where β' and the rate of libration are changed. While these simulated spectra map only moderately well onto the experimental spectra, they do give a good sense of the type of motion occurring with the C_6D_5Cl solvate molecule. At 168 K there is no libration of the solvate molecule. As the temperature is increased from 177 to 198 K the libration angle β' increases from ~22 to ~34°, and it is also necessary to increase the rate of libration from 8×10^4 s^{-1} to 4×10^6 s^{-1}.

From the ^{2}H NMR spectra for the C_6D_5Cl solvate it can be concluded that at the abrupt 188.4 K phase transition the C_6D_5Cl molecules experience the onset of some small motion. Libration about the in-plane C_2 axis starts at this temperature, however the angle of libration is small. It is anticipated that the onset of this librational motion would not contribute to ΔS for the phase transition. Thus, as the plane of the C_6D_5Cl molecule rocks from one side to the other, there is probably no potential-energy barrier.

^{2}H NMR spectra were run at several temperatures for a polycrystalline sample of [Fe(3-OEt-SalAPA)$_2$](ClO$_4$)·C_6D_5Br (figure available in Supplementary Material). At 130 K the

(37) Ok, J.; Vold, R. R.; Vold, R. L.; Etter, M. C. *J. Phys. Chem.* **1989**, *93*, 7618.

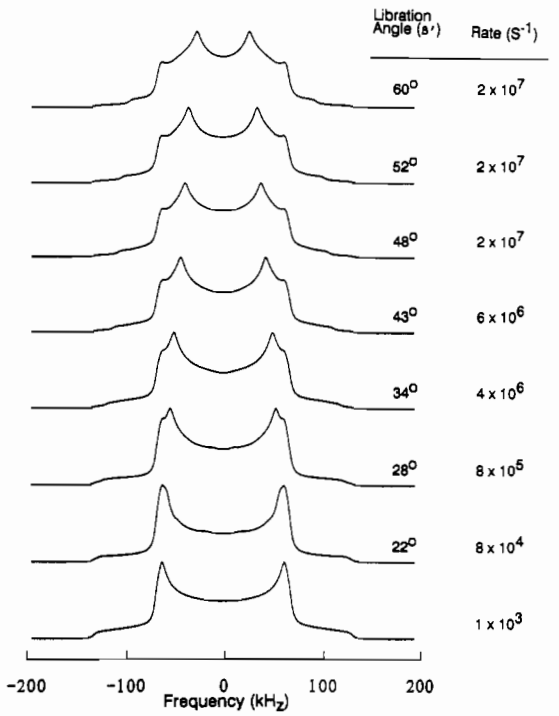

Figure 8. Simulated powder ^2H NMR spectra for $[Fe(3\text{-}OEt\text{-}SalAPA)_2](ClO_4)\cdot C_6D_5Cl$. Various rates of libration (k) about the local C_2 axis of the C_6D_5Cl solvate molecule are employed. The plane of the molecule moves by an angular displacement of β' degrees. The bottom simulation is for a libration angle of 0°.

spectrum is that expected for a static C_6D_5Br solvate molecule. Comparison of this spectrum with the 168 K spectrum (Figure 7) for the C_6D_5Cl solvate shows an interesting difference. The C_6D_5Br spectrum is better resolved and shows structure. Three signals can be seen to make up the positive-velocity 90° "horn". It is clear that separate axial powder patterns are being seen for the ortho, meta, and para deuterons. The three essentially axial powder patterns are shifted by differing amounts of dipole–dipole interactions with a neighboring paramagnetic Fe^{III} cation. It is not necessary to simulate the C_6D_5Br spectra to have a reasonable sense of what is occurring. In the 130–213 K region the C_6D_5Br molecules are static. In the 236–260 K region there is an onset of motion, presumably the same type of libration about a C_2 axis as deduced for the C_6D_5Cl solvate. In fact, in matching the separation in inner horns, the 260 K C_6D_5Br spectrum matches best with the 283 K C_6D_5Cl spectrum. Thus, it appears that the C_6D_5Br solvate molecules experience an onset of motion (angle β' and rate of libration) in a narrower temperature range than the C_6D_5Cl solvates. There is no change at 289 K in the inner "horn" separation. The only thing that happens is that there is a change in the asymmetry of the spectrum. The 288 K phase transition of the C_6D_5Br solvate is only a structural phase transition. Half of the solvate molecules abruptly reorient such their C–Br bond vectors point in a different direction. It is likely that the ΔS value of $\sim$4.7 J K^{-1} mol^{-1} observed for the 288 K phase transition does not have a contribution from the solvate molecule.

Crystal Packing Arrangements. If we are to understand the origin of all the different phases in the solvate series, it is imperative that the crystal packing arrangements be examined. In the series $[Fe(3\text{-}OEt\text{-}SalAPA)_2](ClO_4)\cdot S$ the crystal packings are the same except for subtle differences. In Figure 9 is shown a stereoview of the 298 K ($C2/c$ symmetry) benzene solvate as representative of the series. After thoroughly examining other descriptions, it became clear that the best description of the packing is one of stacks of Fe^{III} cations. Clearly the closest cation–cation contact occurs in these stacks. Figure 9 (upper) shows a stereoview down the cation stacks. Each cation stack is surrounded by a hexagonal arrangement of six columns, where each column consists of alternating stacks of ClO_4^- anions and C_6H_6 solvate molecules. A space-filling stereoview down the cation stacks is shown in Figure 9 (lower). In this drawing the spheres are drawn at the 30% probability level. From this space-filling view it is possible to get a better sense of relative dimensions of cation, anion, and solvate, as well as the spacing between stacks.

As was shown in the preceding paper the bond length to the aziridine ligand, $Fe–N_{az}$, makes the largest change as each cation converts from low spin to high spin. The closest contact between cations in a stack occurs between two aziridine groups, one on each cation. Figure 10 shows a stereoview of this contact as it occurs between two cations in one stack of the C_6H_6 solvate at room temperature. As can be seen in Table III, the proton–proton contacts between these two aziridine groups ranges from 1.87 to 2.06 Å throughout the $[Fe(3\text{-}OEt\text{-}SalAPA)_2](ClO_4)\cdot S$ series. In Table III are also summarized the in-stack Fe···Fe distances, which can be seen to be similar. At room temperature the in-stack Fe···Fe distances are 7.91 Å for the C_6H_6, C_6H_5Cl, and o-$C_6H_4Cl_2$ solvates, with a somewhat larger distance of 7.95 Å for the C_6H_5Br solvate. As the temperature is decreased to $\sim$128–163 K there is $\sim$0.2 Å decrease in these in-stack Fe···Fe distances.

As you view down the cation stack, the $N_{az}–Fe–N_{az}$ direction of each cation is tipped from the stacking direction (Fe atoms are actually aligned in a zigzag fashion). One gauge of this tipping is given by the inter-cation angle $Fe–N_{az}\cdots Fe$. If the Fe atoms in one stack were in-line and the $N_{az}–Fe–N_{az}$ direction was also aligned with the stacking direction, then the angle $Fe–N_{az}\cdots Fe$ would be 180°. As can be seen in Table III, for the 3-OEt-SalAPA$^-$ solvate series this angle is essentially the same ($\sim$114°) for all complexes, independent of temperature.

Since the non-solvated complex, $[Fe(3\text{-}OEt\text{-}SalAPA)_2]ClO_4$, has a considerable more gradual spin-crossover transformation than any of the solvates, it is instructive to look at the packing in this complex. In another paper the 295 K X-ray structure of $[Fe(3\text{-}OMe\text{-}SalAPA)_2]ClO_4$ was reported. In the preceding paper it was established that these two nonsolvated complexes are isostructural, crystallizing at room temperature in the $P\bar{1}$ space group. Again the packing in the two nonsolvated complexes (figure available in Supplementary Material) can be best described as stacks of cations with columns of anions situated approximately midway between the cation stacks. At 295 K the 3-OMe nonsolvated complex has two crystallographically different Fe^{III} cations. From the dimensions and the magnetic susceptibility data one of these cations is 28% high spin, whereas the other is 85% high spin. There are significant differences between the packing of the solvates and the 3-OMe non-solvated complex. Obviously, the $P\bar{1}$ symmetry of the latter means the cations are related to each other only through inversion centers and translation. It is interesting that the removal of the solvate complex reduces the symmetry of the complex. As can be seen in Table III, the in-stack Fe···Fe distance of $\sim$9.0 Å is larger than the $\sim$7.9 Å found for the solvates. There is also one other important difference. In the non-solvated complex at 295 K each stack consists of a single type of Fe^{III} cation. Thus, there are separate stacks of cations which are 28% high spin and those in which the cations are 85% high spin. At low temperatures the C_6H_6, C_6H_5Cl, and C_6H_5Br solvates have been shown to have two different Fe^{III} cations; however, they are assembled in alternating stacks.

In summary, upon addition of a solvate molecule the cations in a given stack are forced together such that the in-stack Fe···Fe distance is reduced by $\sim$1 Å. In each stack the cations reorient upon solvation so that the EtO···EtO intercation interaction is minimized. This reorientation of cations in each stack leads to space developing between stacks, space into which the solvate molecules move. Also, the addition of solvate molecules considerably reduces the direct contact between cations in neighboring stacks. The solvate molecules act as a spacer between the cation stacks. They become the means of communication between stacks.

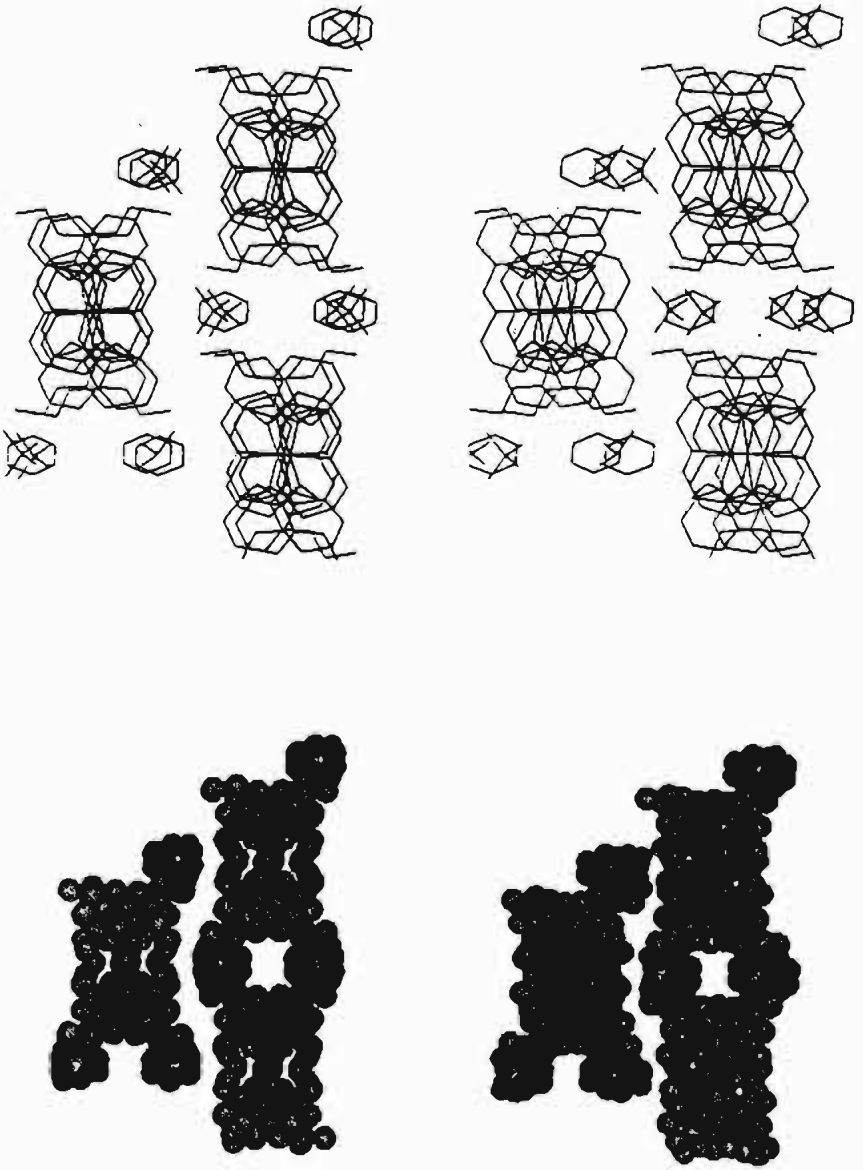

Figure 9. Stereoview of $C2/c$ symmetry (298 K) $[Fe(3\text{-}OEt\text{-}SalAPA)_2](ClO_4)\cdot C_6H_6$: (upper) stick drawing viewed down the stacks of Fe^{III} complexes; (lower) space-filling model of the same down-the-stack view.

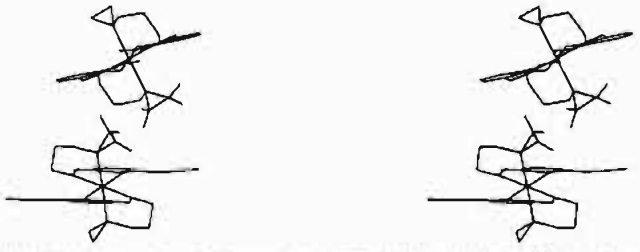

Figure 10. Stereoview of two cations of $[Fe(3\text{-}OEt\text{-}SalAPA)_2](ClO_4)\cdot C_6H_6$ at 298 K. The two cations occur in one stack and the view is perpendicular to the stacking direction.

Obviously in the 3-OEt solvate series it is the exact positioning of the solvate molecule which determines the space group symmetry of a given solvated complex. If the solvate molecules undergo a change in position, then a different phase results.

Structural Phase Transition of C_6H_5Cl and C_6H_5Br Solvates. The C_6H_5Br solvate has an abrupt phase transition with $\Delta S \simeq R \ln 2$ at 288.3 K. The spin-crossover transformation occurs independently of this phase transition. The C_6H_5Cl solvate also exhibits an abrupt phase transition. However, this 188.4 K phase transition involves the spin-crossover change. It will be shown in this section that there is also a structural change occurring in this abrupt 188.4 K phase transition.

Table III. Intrastack Distances and Angles for the $[Fe(3\text{-}OEt\text{-}SalAPA)_2]ClO_4\cdot S$ and $[Fe(3\text{-}OMe\text{-}SalAPA)_2]ClO_4\cdot S$ Solvate Series

complex	T, K	Fe- - -Fe,[a] Å	N(az)- - -N(az),[b] Å	Fe, Fe, N(az),[c] deg
		$[Fe(3\text{-}OEt\text{-}SalAPA)_2](ClO_4)\cdot S$		
$o\text{-}C_6H_4Cl_2$	298	7.91	1.87	113.8
C_6H_5Br	298	7.95	2.06	114.4
C_6H_5Br	163	7.77	2.04	114.7
C_6H_5Cl	298	7.91	2.02	114.2
C_6H_5Cl	158	7.69	2.01	114.4
C_6H_6	298	7.91	1.90	113.8
C_6H_6	128	7.70	1.93	113.8
		$[Fe(3\text{-}OMe\text{-}SalAPA)_2](ClO_4)\cdot S$		
no solvate S	298	9.04	2.15/3.37	143.1

[a] Distance between two iron ions in neighboring cations in a stack. [b] Closest proton-proton distance between two aziridine moieties on neighboring complexes in a stack. [c] Angle characterizing relative tip of Fe complexes in a stack, see text for description.

The temperature dependence of the conversion of the C_6H_5Cl solvate from $P2_1/a$ at 158 K to $P2_1/c$ at room temperature was examined in detail. A single crystal was mounted and the space group and unit cell parameters determined at nine different

Table IV. Temperature Dependence[a] of Unit Cell Parameters and Space Group for $[Fe(3\text{-}OEt\text{-}SalAPA)_2](ClO_4)\cdot C_6H_5Cl$

T, K	space group	a, Å	b, Å	c, Å	β, deg	V, Å³
190	$P2_1/c$	13.744(3)	17.611(6)	15.588(5)	110.31(2)	3538(2)
185	$P2_1/a$	13.649(3)	17.517(8)	16.915(6)	119.83(2)	3509(4)
180	$P2_1/a$	13.650(3)	17.518(8)	16.916(7)	119.83(2)	3509(2)
188	$P2_1/a$	13.667(3)	17.538(9)	16.942(7)	119.75(2)	3526(3)
190	$P2_1/c$	13.766(6)	17.623(9)	15.605(9)	110.43(5)	3547(3)
189	$P2_1/c$	13.766(6)	17.624(9)	15.604(9)	110.42(4)	3548(3)
173	$P2_1/_a$	13.630(5)	17.490(10)	15.539(9)	109.58(4)	3491(3)
176	$P2_1/a$	13.636(6)	17.490(10)	15.550(10)	109.60(5)	3496(4)
178	$P2_1/a$	13.642(6)	17.497(1)	15.563(9)	109.61(4)	3499(3)
179	$P2_1/a$	13.643(3)	17.512(9)	16.920(7)	119.83(2)	3506(2)

[a] Temperatures are listed in the order obtained experimentally.

Table V. Unit Cell Parameters for $[Fe(3\text{-}OEt\text{-}SalAPA)_2](ClO_4)\cdot C_6H_5Br$

T, K	space group	a, Å	b, Å	c, Å	β, deg	V, Å³
290	$P2_1/c$	13.84(2)	17.95(5)	15.83(6)	110.0(3)	3664.1(3)
284	$P2_1/a$	13.79(5)	17.68(9)	15.83(3)	109.5(6)	3640.1(4)
273	$P2_1/a$	13.78(8)	17.66(6)	15.81(5)	109.5(3)	3631.7(5)
213	$P2_1/a$	13.72(1)	17.55(9)	15.69(7)	109.4(0)	3568.1(4)
148	$P2_1/a$	13.61(7)	17.49(0)	15.49(2)	109.0(8)	3486.3(2)

temperatures from 190 to 173 K. The temperature was varied in the order listed in Table IV. As can be seen the space group was found to be $P2_1/c$ at 190 and 189 K. There is a very abrupt change to another phase described as $P2_1/a$ at 188 K. This phase persists in the 188 to 179 K range. However, upon decreasing the temperature from 179 to 178 K there is a second abrupt change where the space group remains as $P2_1/a$, but the β angle abruptly decreases from ~119° in the 188–179 K range to ~110° in the 178–158 K range. The observation of two structural changes at ~188 and ~178 K is in agreement with the C_P data for the C_6H_5Cl solvate which shows a sharp maximum in ΔC_P at 188.4 K and a broad peak at ~177 K.

It should be noted that the $P2_1/a$ setting is a crystallographically nonstandard setting of the $P2_1/c$ space group. By describing the low temperature structure as $P2_1/a$, it is possible to maintain the convention of having the a-axis of the unit cell as the shortest and the c-axis as the longest unit cell dimension. Structurally, this allows for a more direct comparison between the low- and room-temperature structures. The cations assume the same relative positions in the two space groups. The structural differences between the $P2_1/a$ and $P2_1/c$ phases are due to the repositioning of solvate molecules. In panels A and B of Figure 11 are given stereo packing diagrams of the 158 and 295 K C_6H_5Cl structures, respectively. It can be seen that in both diagrams the cations and anions remain in the same relative positions. Each diagram gives a view looking down two cation stacks, where each stack is pictured with two Fe^{III} cations. In each diagram four C_6H_5Cl solvate molecules are numbered 1–4 and two ethoxy arms, each belonging to a different cation in one stack, are labeled a and b. In the conversion from the low-temperature $P2_1/a$ setting to the $P2_1/c$ setting at room temperature, solvates 2 and 4 reorient their C–Cl bond axes. In reference to solvate 2, this involves a change from an orientation in which the solvate chlorine atom is directed toward ethoxy arm a of the "lower" cation to an orientation in which the chlorine atom is directed toward the ethoxy arm labeled b on the "upper" cation. In fact, each solvate molecule is surrounded by several cations. The closest contacts felt by the C_6H_5Cl solvate molecules are with the ethoxy arm of nearby cations. The chlorine atom of the solvate molecule experiences the shortest contact distance with an ethoxy arm of a cation.

Finally, it was instructive to examine in closer detail what happens to a single crystal of the C_6H_5Br solvate when it undergoes the abrupt phase transition at 288 K. In Table V are given the space group and unit cell parameters measured for a single crystal as it was examined at five temperatures from 148 to 290 K. It can be seen that the crystal abruptly changes from $P2_1/c$ to $P2_1/a$ when the crystal was cooled from 290 to 284 K. Furthermore, in contrast to the crystal of the C_6H_5Cl solvate there was no evidence of a second $P2_1/a$ phase. Only a $P2_1/a$ setting with $\beta \simeq 109°$ was seen.

Phase Diagram. In Table VI are summarized the different phases found for the complexes in the 3-OEt and 3-OMe solvate series. Even though the one 3-OMe complex has the same basic arrangement of stacks of Fe^{III} cations found for the 3-OEt series, it is not simple to position the 3-OMe phase V on a phase diagram with the 3-OEt complexes. In the 3-OEt series we have identified four different phases. A qualitative phase diagram for the 3-OEt-complexes can be constructed as shown in Figure 12. In this diagram at a given temperature each phase is characterized by an internal pressure, which is just a qualitative measure of the average intermolecular interactions present in each compound. The contact of two aziridine groups, one on each of two Fe^{III} cations, largely determines the intermolecular interactions between Fe^{III} cations in each stack. These intrastack interactions are modulated by the solvate molecule S (see Table III). Obviously, the nature of the solvate molecule S determines the intermolecular interactions between Fe^{III} complexes in neighboring stacks.

The solid lines on the phase diagram indicate the boundaries between the phases I, II, III, and IV. The three horizontal dashed lines are drawn to indicate which phases are accessed by the C_6H_5Br, C_6H_5Cl, and C_6H_6 solvates. At low temperatures, $[Fe(3\text{-}OEt\text{-}SalAPA)_2](ClO_4)\cdot C_6H_5Br$ is in phase II, and upon heating there is clear evidence from X-ray diffraction and C_P data of a structural phase transition abruptly occurring at 288.3 K. Thus, the lowest dashed line indicates that this C_6H_5Br solvate converts from phase II to phase III at ~288 K.

The middle dashed line is drawn to summarize the observations on the C_6H_5Cl solvate. At low temperatures it is in phase II, and from X-ray diffraction data we know that with increasing temperature the C_6H_5Cl solvate converts at ~177 K to phase I. It exists in this phase only over a ~10-deg range, for at 188.4 K it converts abruptly to phase III, the same phase that the C_6H_5Br solvates assumes at room temperature. It should be noted that there are several well documented cases of compounds that exist in one phase for a very narrow temperature range. For example, two C_P peaks at 436.5 and 437.8 K have been reported for $NaNO_2$.[38] At room temperature $NaNO_2$ is in a ferroelectric phase and converts to an antiferroelectric phase at 436.5 K and then finally to a paraelectric phase above 437.8 K. The antiferroelectric phase is only stable for a range of 1.3 deg at 1 atm of pressure. The antiferroelectric character of this 1.3-deg range phase has been established theoretically and experimentally to be due to a sinusoidal modulation of the electric moments of the NO_2^- ions along the a axis of the crystal.[39,40]

It is perhaps more difficult to know the phases of the 3-OEt benzene solvate. The top horizontal line suggests that this compound exists as phase I at low temperatures and converts at higher temperatures to phase IV. In passing we note that the o-$C_6H_4Cl_2$ solvate also seems to take this same phase IV structure at room temperature.

Influence of Phase Transitions on Spin-Crossover Transformations. With all of the above data is it appropriate to ask what the relationship of the observed phase transition is to the spin-crossover transformations. From Figure 1 in the preceding paper it is clear that as the solvate molecule S in $[Fe(3\text{-}OEt\text{-}SalAPA)_2](ClO_4)\cdot S$ is changed, not only does the shape of the μ_{eff} versus temperature curve change, but the critical temperature T_C also changes. Some level of cooperativity exists in any given phase transition. It is clear from the C_P data that the C_6H_5Cl and C_6H_5Br solvate molecules each exhibit one phase transition

(38) Sakiyama, M.; Kimoto, A.; Seki, S. *J. Phys. Soc. Jpn.* **1965**, *20*, 2180.
(39) Yamada, Y.; Shibuya, I.; Hoshino, S. *J. Phys. Soc. Jpn.* **1963**, *18*, 1594.
(40) Hosino, S.; Motegi, H. *Jpn. J. Appl. Phys.* **1967**, *6*, 708.

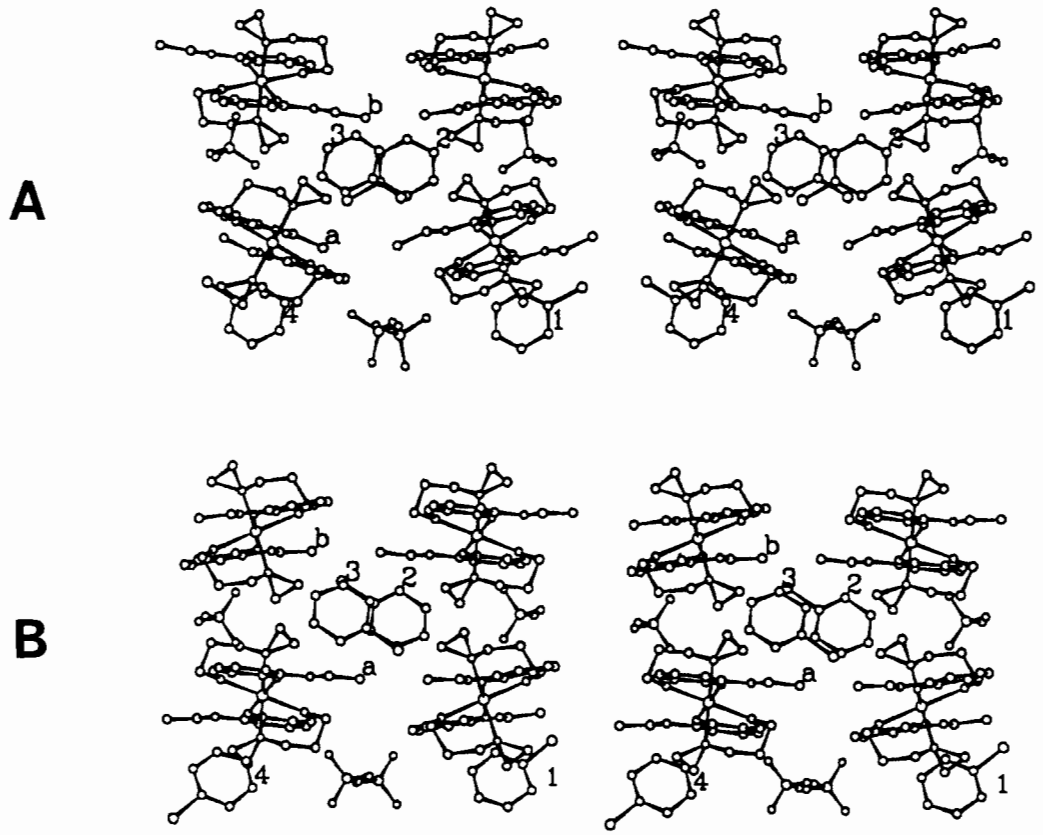

Figure 11. Stereoview of the packing in $[Fe(3\text{-}OEt\text{-}SalAPA)_2](ClO_4)\cdot C_6H_5Cl$ as viewed down the stacks of Fe^{III} cations: (A) $P2_1/a$ symmetry structure at 158 K; (B) $P2_1/c$ symmetry structure at 295 K.

Table VI. Crystallographic Data for $[Fe(3\text{-}OEt\text{-}SalAPA)_2](ClO_4)\cdot S$ and $[Fe(3\text{-}OMe\text{-}SalAPA)_2](ClO_4)\cdot S$ Solvate Series

complex	T, K	space group	phase	no. of unique cation sites	inversion sym for cation
		$[Fe(3\text{-}OEt\text{-}SalAPA)_2](ClO_4)\cdot S$			
C_6H_6	128	$P2_1/c$	I	2	no
C_6H_5Cl	<177	$P2_1/a$	II	2	no
C_6H_5Cl	178–188	$P2_1/a$	I	2	no
C_6H_5Br	163	$P2_1/a$	II	2	no
C_6H_5Cl	189–295	$P2_1/c$	III	1	no
C_6H_5Br	295	$P2_1/c$	III	1	no
$o\text{-}C_6H_4Cl_2$	295	$C2/c$	IV	1	yes
C_6H_6	295	$C2/c$	IV	1	yes
		$[Fe(3\text{-}OMe\text{-}SalAPA)_2](ClO_4)\cdot S$			
no solvate	295	$P\bar{1}$	V	2	yes

with appreciable cooperativity. These phase transitions are abrupt because of long range order, which reflects the presence of appreciable intermolecular interactions. One critical question is whether there is any cooperativity in the spin-crossover transformations observed for the 3-OEt solvate complexes. At the outset we can easily say that there is clearly appreciable cooperativity in the spin-crossover transformation for the C_6H_5Cl solvate complex.

One possible way to analyze the spin-crossover transformation in the solid state is to see whether the μ_{eff} versus temperature data for a given compound can be least-squares fit by assuming that there is an equilibrium present,

$$\underset{(1-f)}{\text{low-spin}} \overset{K}{\rightleftharpoons} \underset{(f)}{\text{high-spin}} \qquad (6)$$

where f represents the fraction of high-spin Fe^{III} complexes present at any temperature. The equilibrium constant K is given by

$$K = f/(1-f) \qquad (7)$$

The thermodynamic relationship between K, ΔG, ΔH, and ΔS is given by

$$\ln K = -\Delta G/RT = -\Delta H/RT + \Delta S/R \qquad (8)$$

By substituting K in eq 8 with eq 7 the following equation can be obtained:

$$f = \exp(-\Delta H/RT + \Delta S/R)/[1 + \exp(-\Delta H/RT + \Delta S/R)] \qquad (9)$$

A computer program was used to least-squares fit the μ_{eff} versus temperature data of Figure 1 in the preceding paper (μ_{eff} values are readily converted to f values). It was found that, except for the data for the C_6H_5Cl solvate, good fits of the data were obtained for the C_6H_6, C_6H_5Br, and $o\text{-}C_6H_4Cl_2$ solvates.

Figure 13 shows the fit of the data for the C_6H_5Br and C_6H_6 solvate data (figures are available in the supplementary material

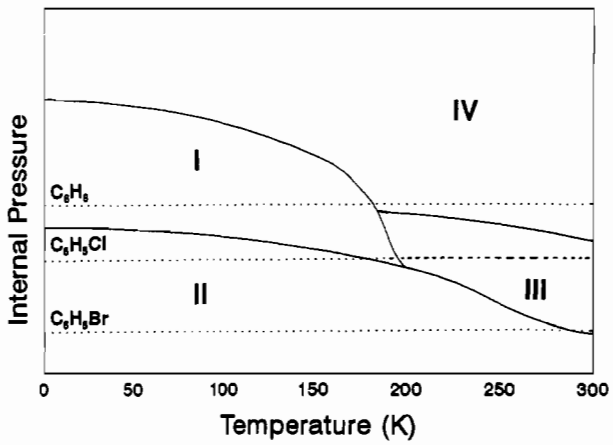

Figure 12. Qualitative phase diagram to summarize the four phases found for the complexes in the $[Fe(3\text{-}OEt\text{-}SalAPA)_2](ClO_4)\cdot S$ series. "Internal pressure" is a qualitative measure of average intermolecular interactions. Dashed horizontal lines are drawn for three of the complexes to show phase transitions that occur at various temperatures.

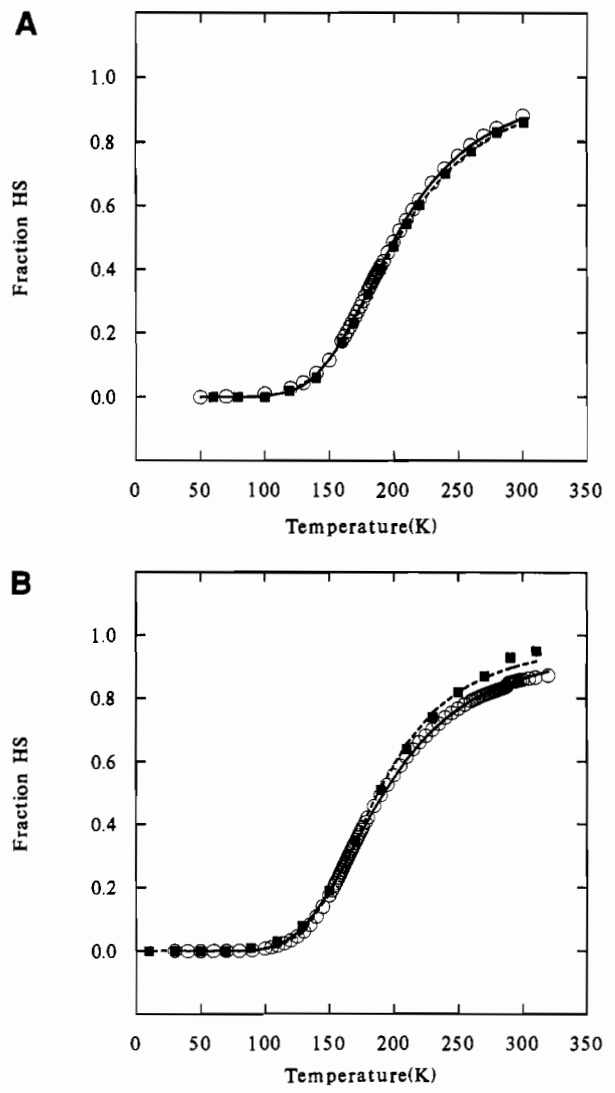

Figure 13. Plots of the fraction (f) of high-spin complexes versus temperature for (A) [Fe(3-OEt-SalAPA)$_2$](ClO$_4$)·C$_6$H$_5$ and (B) [Fe(3-OEt-SalAPA)$_2$](ClO$_4$)·C$_6$H$_5$Br. The f values were calculated from susceptibility data. For each of the two compounds two different data sets are presented. The lines result from least-squares fits to eq 9.

for the fits of the C$_6$H$_5$Cl and o-C$_6$H$_4$Cl$_2$ solvate). In the case of the C$_6$H$_6$ solvate a very good fit of the μ_{eff} versus temperature data is possible assuming that an equilibrium is present and using the parameters ΔH and ΔS. The μ_{eff} data given in Figure 1 of the preceding paper are quite typical susceptibility data where the full data set was collected in a total period of 5–6 h. Fitting these data gave ΔH = 9.71 kJ mol^{-1} and ΔS = 47.5 J K^{-1} mol^{-1} for the C$_6$H$_6$ solvate. By comparison with the data in Table I, it can be seen that the ΔH and ΔS values obtained by fitting the susceptibility data for the C$_6$H$_6$ solvate are appreciably larger than the much more precisely known ΔH and ΔS values evaluated from the heat capacity data.

In Table VII are collected the ΔH and ΔS values evaluated by fitting the susceptibility data for all four of the 3-OEt solvate complexes. In Figure 13B it can be seen that the fit (dashed line) of the C$_6$H$_5$Br solvate data is good except at temperatures approaching room temperature. A comparison of ΔH and ΔS values from susceptibility data (Table VII) with those from heat capacity data (Table I) show that, except in the case of the o-C$_6$H$_4$Cl$_2$ solvate, the former values are significantly larger. In the case of the o-C$_6$H$_4$Cl$_2$ solvate the two sets of ΔH, ΔS values are quite close. A figure in the supplementary material shows that the overall shape of the μ_{eff} versus temperature curve for the C$_6$H$_5$Cl solvate cannot be well fit. There is an abrupt increase in the fraction of high spin complexes near the 188.4 K phase transition.

Table VII. Total Enthalpy (ΔH) and Total Entropy (ΔS) Changes Evaluated by the Least-Squares Fitting to the Magnetic Susceptibility Data for the [Fe(3-OEt-SalAPA)$_2$](ClO$_4$)·S Complexes[a]

solvate S	data set	ΔH, kJ/mol	ΔS, J/(K mol)
C$_6$H$_6$	1	9.71	47.5
	2	9.86	48.9
C$_6$H$_5$Cl	1	11.88	64.6
	2	13.00	68.5
C$_6$H$_5$Br	1	9.51	50.7
	2	8.21	42.7
o-C$_6$H$_4$Cl$_2$	1	5.52	39.9
	2	5.12	35.9

[a] Two data sets were determined for each compound. The Data set 1 was run over a shorter time period than data set 2; see text for details.

There are several reasons why the ΔH, ΔS values evaluated from susceptibility data do not agree with those determined in the heat capacity experiment. First, to evaluate ΔH and ΔS from the susceptibility data it is assumed that ΔH and ΔS are independent of temperature. Second, as indicated above the complete susceptibility data set for each compound was collected in a total period of 5–6 h. On the other hand considerably more time was taken to collect the heat capacity data set for each compound. In the adiabatic calorimetry experiment the sample is first cooled to ~13 K and allowed to reach thermal equilibrium (several hours). Increments of current to a heating element are supplied and after each increment enough time is allowed to approach closely thermal equilibration. In the region of heat capacity effects (*i.e.*, bumps in ΔC_P versus temperature curves) it may take as long as 1.5–2.0 h to closely approach equilibrium after an increment which only raises the sample temperature by 0.5 deg. As a result it takes days to collect a data set for a compound.

Additional susceptibility data were collected for polycrystalline portions of the heat capacity samples of each of the four 3-OEt solvates. A period of 12–14 h was employed to collect the data for the C$_6$H$_6$ and C$_6$H$_5$Cl solvates, and ~24 h was employed per compound to recollect data for the C$_6$H$_5$Br and o-C$_6$H$_4$Cl$_2$ solvates. These data are also shown in the figures. In Figure 13A it can be seen that the two data sets for the C$_6$H$_6$ solvate give essentially superimposable f versus T curves. Fitting of the second data gives ΔH, ΔS values (Table VII) which are quite similar to those evaluated by fitting the first data set.

In contrast, the 24 h susceptibility data set for the C$_6$H$_5$Br solvate (Figure 13B) does not track well at the higher temperatures the first data set which was obtained in ~5 h. In passing we note that the second data set does show a kink corresponding to the structural phase transition at 288 K. Fitting of the second data set gives different values for ΔH and ΔS (Table VII). The values of ΔS decreased from 50.7 to 42.7 J K^{-1} mol^{-1} with a smaller decrease of ΔH from 9.51 to 8.21 kJ mol^{-1}. The ΔH, ΔS values obtained from the second data set are much closer to the higher precision values evaluated from the C_P data. Smaller ΔH, ΔS values were also found for the second susceptibility data set compared to the first data set for the o-C$_6$H$_4$Cl$_2$ solvate, however, the reverse trend was noted (Table VII) for the C$_6$H$_5$Cl solvate.

There are a couple of conclusions which can be made about the above susceptibility data. First, there is a dependence in three cases of the shape of the f versus T curve on the rate of data collection. This is evidence for at least a weak cooperativity in spin-crossover transformation for the C$_6$H$_5$Br and o-C$_6$H$_4$Cl$_2$ solvates. Strong cooperativity of spin-crossover transformation has already been established for the C$_6$H$_5$Cl solvate. Second, it is clear that least-squares fitting of susceptibility data is not a good way to evaluate ΔH and ΔS. In fact, it is not clear whether the ability to fit susceptibility data is a good criterion to establish whether or not there is any cooperativity in the spin-crossover transformation. In all four cases ΔS evaluated from the susceptibility data is larger than the ΔS value from the heat capacity data. If there is a spin-equilibrium present, ΔS evaluated

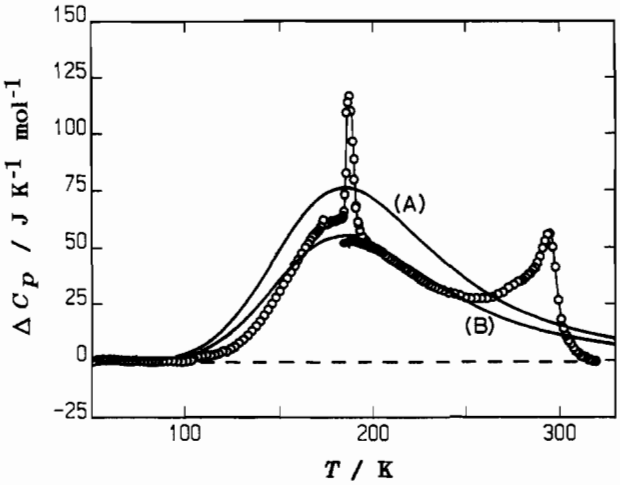

Figure 14. Plot of excess heat capacity, ΔC_P, versus temperature for $[Fe(3\text{-}OEt\text{-}SalAPA)_2](ClO_4)\cdot C_6H_6$. The solid lines A and B are theoretical lines calculated from eq 10. See text for parameters.

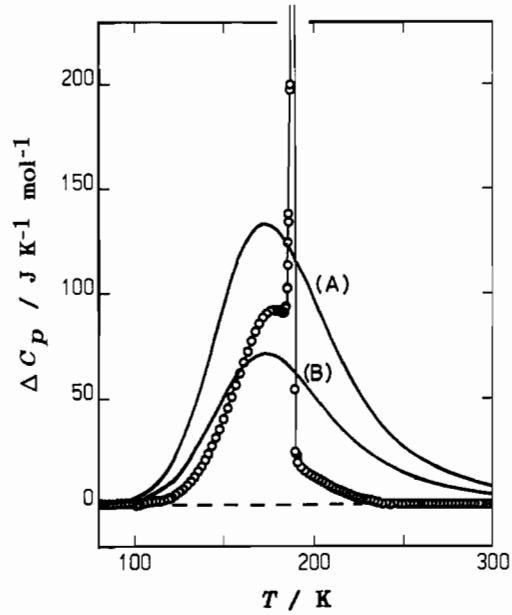

Figure 15. Plot of excess heat capacity, ΔC_P, versus temperature for $[Fe(3\text{-}OEt\text{-}SalAPA)_2](ClO_4)\cdot C_6H_5Cl$. The solid lines A and B are theoretical lines calculated from eq 10. See text for parameters.

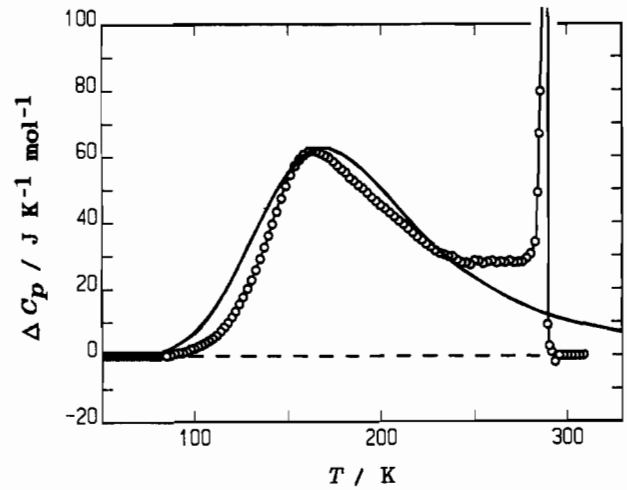

Figure 16. Plot of excess heat capacity, ΔC_P, versus temperature for $[Fe(3\text{-}OEt\text{-}SalAPA)_2](ClO_4)\cdot C_6H_5Br$. The solid line is a theoretical line calculated from eq 10. The values of ΔH and ΔS were taken from fitting the second magnetic susceptibility data set.

from the susceptibility data for each complex should be equal to an electronic entropy term ($R \ln 3 = 9.13$ J K^{-1} mol^{-1} for conversion from $^2T_2$ to $^6A_1$ complex) plus a term reflecting a change in the vibrational quanta for the Fe^{III} complex. The sum should always be less than the ΔS value evaluated from the heat capacity. This is the case because the latter includes contributions from other sources such as structural phase transitions or the onset of motion of the ClO_4^- or even the ethoxy arm of the ligand.

Probably the best way to evaluate whether there is any cooperativity in the spin-crossover transformation is to simulate the appearance of the ΔC_P versus T experimental data. Since the total enthalpy change realized by converting from the low- to high-spin state is ΔH, the acquisition enthalpy at T is $(f\Delta H)$. The excess heat capacity (ΔC_P) is therefore given by

$$\Delta C_P = \mathrm{d}(f\Delta H)/\mathrm{d}T = \frac{[(\Delta H)^2/RT^2][\exp(-\Delta H/RT + \Delta S/R)]}{[1 + \exp(-\Delta H/RT + \Delta S/R)]^2} \quad (10)$$

The different values of ΔH and ΔS for a given compound can be used to calculate a ΔC_P versus temperature curve.

In Figure 14 are shown the ΔC_P versus temperature data for the C_6H_6 solvate. Curve A was calculated by using $\Delta H = 9.71$ kJ mol^{-1} and $\Delta S = 47.5$ J K^{-1} mol^{-1} as evaluated from the first susceptibility data set. As can be seen, curve A mimics the broad main part of the ΔC_P versus temperature data set. However, curve A falls considerably above the experimental data. A better correspondence is found for curve B, which was calculated, as an approximation, by reducing the ΔC_P obtained from eq 10 with the factor of $\Delta H(\mathrm{cal})/\Delta H(\mathrm{mag})$, where $\Delta H(\mathrm{cal}) = 7.08$ kJ mol^{-1} is the value from the C_P data while $\Delta H(\mathrm{mag}) = 9.71$ kJ mol^{-1} is the value from the susceptibility data. There seems to be two phase transitions at 187 and 295.3 K which occur relatively independently of the spin-crossover transformation. At most there is only a very weak cooperativity which may be evidenced by the small deviations of curve B from the "broad" part of the experimental data.

The situation for the C_6H_5Cl solvate is more interesting; see Figure 15. Curve A was calculated with $\Delta H = 11.88$ kJ mol^{-1} and $\Delta S = 64.6$ J K^{-1} mol^{-1} as per fitting the first susceptibility data set, and curve B results from the same reduction procedure as in the case of the C_6H_6 solvate by employing the smaller ΔH value (6.34 kJ mol^{-1}) from the C_P data. Although curve B follows reasonably well the ΔC_P experimental data at low temperatures, agreement is poor near to the phase transition at 188.4 K and at higher temperatures. It is clear that the cooperativity between the spin-crossover transformation and the structural change is strong. When half of the solvate molecules reorient in the structural change, there must be enough of a volume change in the crystal so that a large fraction of the Fe^{III} complexes can also cooperatively convert from a low- to a high-spin state.

As can be seen in Figure 16, a reasonable simulation of the ΔC_P curve can be had by employing the ΔH (=8.21 kJ mol^{-1}) and ΔS (=42.7 J K^{-1} mol^{-1}) values from fitting the second susceptibility data set obtained over a period of ~24 h for the C_6H_5Br solvate. It can be concluded that the spin-crossover transformation for most of the Fe^{III} complexes in this sample proceeds in an equilibrium manner. The shape of the theoretical curve in Figure 16 does not match exactly the experimental data. This may be due to several reasons. It is clear that ΔH and/or ΔS, as evaluated with the susceptibility data, are temperature dependent, however the magnitudes of the temperature dependencies are not known. The theoretical curve in Figure 16 is generally broader than the experimental curve. Also, in the region of ~230 to ~280 K the theoretical curve deviates appreciably from the experimental data. All of the deviations may reflect the presence of long- and short-range order in the spin-crossover transformation. It is clear that the abrupt structural phase transition at 288.3 K does not couple at all with the spin-crossover transformation. It may be that the intermolecular interactions in the C_6H_5Br solvate crystal are such

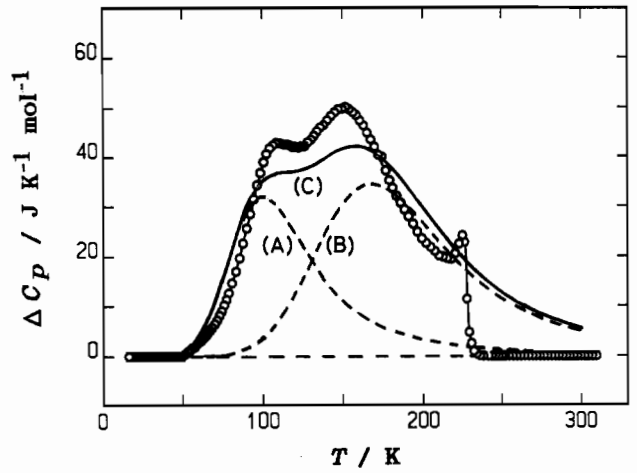

Figure 17. Plot of excess heat capacity, ΔC_P, versus temperature for $[Fe(3\text{-}OEt\text{-}SalAPA)_2](ClO_4)\cdot C_6H_4Cl_2$. The dashed lines A and B were calculated by means of eq 10 with ΔH and ΔS given in the text. The curve C results from a superposition of curves A and B. It is assumed there are two different Fe^{III} cations which undergo their spin-crossover transformations at different temperatures.

that it requires a much higher temperature (288.3 *vs* 188.4 K) than the C_6H_5Cl solvate crystal to carry out the structural phase transition. The C_6H_5Br solvate molecules require more space so that half of them can reorient. By 288.3 K most of the Fe^{III} cations in the C_6H_5Br solvate have *in an equilibrium fashion* converted to the high-spin state. Thus, when the C_6H_5Cl solvate crystal makes its structural reorientation at 188.4 K, many of the Fe^{III} cations are still in the low-spin state. The sudden increase in volume occurring at 188.4 K for the C_6H_5Cl solvate crystal encourages the Fe^{III} cations to cooperatively convert to the high-spin state.

Finally, the interesting case of the $o\text{-}C_6H_4Cl_2$ solvate is highlighted in Figure 17. There are two broad peaks in the ΔC_P versus temperature data. Obviously, it is not at all possible to fit the experimental data with a simple equilibrium between a low-spin state and a high-spin state. If the ΔH and ΔS values from fitting the susceptibility data are used with eq 9, only one maximum in ΔC_P versus T is obtained. In Figure 17 is given a suggestion of how to explain the observed ΔC_P data. The experimental curve can be simulated by assuming that at low temperatures there are two different Fe^{III} cations in the crystal in equal amounts. As the temperature is increased, one of the types of Fe^{III} cations makes the transformation before the other type of Fe^{III} cation. This would give two peaks in the ΔC_P data set. Curve C was calculated as the summation of curves A and B. Curve A was calculated with ΔH = 4.9 kJ mol^{-1} and ΔS = 43 J K^{-1} mol^{-1}, whereas curve B was calculated with ΔH = 8.5 kJ mol^{-1} and ΔS = 45 J K^{-1} mol^{-1}. Thus, it is suggested that the $o\text{-}C_6H_4Cl_2$ solvate crystal is comprised of two different Fe^{III} cations which exhibit the spin-crossover transformation at different temperatures.

The presence of Fe^{III} complexes at two crystallographically different sites which undergo the spin-crossover transformation at different temperations has been noted before. In fact, the structure of $[Fe(3\text{-}OMe\text{-}SalAPA)_2](ClO_4)$ shows that at 298 K there are two different Fe^{III} cations. From the bond lengths it was concluded that the cations at site A are 28% high spin, whereas those at site B are 85% high spin. These values were found to be consistent with the magnetic susceptibility of this complex at 298 K. The two different Fe^{III} ions sit at different crystal sites and in effect feel different crystal fields, *i.e.*, "internal pressures".

Concluding Comments. The detailed nature of the spin-crossover transformation in the $[Fe(3\text{-}OEt\text{-}SalAPA)_2](ClO_4)\cdot S$ series has been studied, where the solvate molecule S is either C_6H_6, C_6H_5Cl, C_6H_5Br, or $o\text{-}C_6H_4Cl_2$. Through a combination of single-crystal X-ray diffraction and heat-capacity measurements it was found that these complexes exist in five different phases. The C_6H_5Cl solvate, in fact, converts as the temperature is increased from phase II to phase I at ~177 K and finally to phase III at ~188 K. The second phase transition is abrupt and involves a large entropy gain. Examination of the packing arrangements of the above compounds shows that they all have the same arrangement. There are stacks of Fe^{III} cations where the closest contact is between aziridine moieties of the ligands. Each cation stack is surrounded by columns of ClO_4^- anions and S solvate molecules. Addition of a S solvate molecule or increasing the size of the S molecule leads to a decrease in the intrastack Fe···Fe distance. It is clear that the solvate molecule affects intermolecular interactions both within the stacks of Fe^{III} cations and also between Fe^{III} cations in neighboring stacks.

Variable-temperature solid-state ^2H NMR was used to examine the C_6D_6, C_6D_5Cl, and C_6D_5Br solvates in the 3-OEt series. ^2H NMR signals were readily observed for these paramagnetic solids. Throughout the 147–295 K region the C_6D_6 solvate molecules were found to undergo rapid rotation about a local C_6 axis normal to the plane of the molecule. At the higher temperatures there is an increasing wobbling of the normal axis of the C_6D_6 molecule. A similar type of wobbling about local C_2 axes were detected for the C_6D_5Cl and C_6D_5Br solvate molecules. There was no evidence in any of the three solvates that the solvate molecules underwent an abrupt increase in motion at temperatures which correspond to the phase transitions detected by means of the heat capacity data.

The shapes of the fraction of high spin versus temperature (magnetic susceptibility) and ΔC_P versus temperature curves for the four 3-OEt solvates were examined in detail. The main question addressed was: Is there any cooperativity in the spin-crossover transformation? It was also of interest to understand any possible relationship between the spin-crossover transformation and the observed phase transitions. Three main conclusions were made. There is strong cooperativity of the spin-crossover transformation in the C_6H_5Cl solvate. It occurs in a first-order phase transition which also involves a structural rearrangement where half of the C_6H_5Cl solvate molecules reorient. Second, if there is cooperativity in the spin-crossover transformation in the other three 3-OEt solvates, it is very weak. Some evidence for weak cooperativity was found in the fact that the μ_{eff} versus temperature data depend on the rate of data collection; also, the appearance of ΔC_P versus temperature curves gives some evidence for a very weak cooperativity. Third, the $o\text{-}C_6H_4Cl_2$ solvate must have two different Fe^{III} cations which undergo the spin-crossover change at different temperatures as evidenced by two broad peaks in the ΔC_P versus temperature curve.

Acknowledgment. We are grateful for funding from National Institutes of Health Grant HL13652 (D.N.H.) and National Science Foundation Grant CHE-9115286 (D.N.H.). D.N.H. and M.S. are also grateful for a travel grant from the National Science Foundation (INT-9016821) and the Japan Society for the Promotion of Science.

Supplementary Material Available: Figures showing the variable-temperature ^2H NMR spectra for polycrystalline $[Fe(3\text{-}OEt\text{-}SalAPA)_2](ClO_4)\cdot C_6D_5Br$ and a stereoview of the packing in the crystal of $[Fe(3\text{-}OMe\text{-}SalAPA)_2](ClO_4)$ at 295 K (3 pages). Ordering information is given on any current masthead page.